

# Communication-Efficient Federated Learning via Quantized Compressed Sensing

Yongjeong Oh, Namyoon Lee, Yo-Seb Jeon, and H. Vincent Poor

## Abstract

In this paper, we present a communication-efficient federated learning framework inspired by quantized compressed sensing. The presented framework consists of gradient compression for wireless devices and gradient reconstruction for a parameter server (PS). Our strategy for gradient compression is to sequentially perform block sparsification, dimensional reduction, and quantization. Thanks to gradient sparsification and quantization, our strategy can achieve a higher compression ratio than one-bit gradient compression. For accurate aggregation of the local gradients from the compressed signals at the PS, we put forth an approximate minimum mean square error (MMSE) approach for gradient reconstruction using the expectation-maximization generalized-approximate-message-passing (EM-GAMP) algorithm. Assuming Bernoulli Gaussian-mixture prior, this algorithm iteratively updates the posterior mean and variance of local gradients from the compressed signals. We also present a low-complexity approach for the gradient reconstruction. In this approach, we use the Bussgang theorem to aggregate local gradients from the compressed signals, then compute an approximate MMSE estimate of the aggregated gradient using the EM-GAMP algorithm. We also provide a convergence rate analysis of the presented framework. Using the MNIST dataset, we demonstrate that the presented framework achieves almost identical performance with the case that performs no compression, while significantly reducing communication overhead for federated learning.

## Index Terms

Federated learning, quantized compressed sensing, distributed stochastic gradient descent, gradient compression, gradient reconstruction

This paper will be presented in part at the 2021 IEEE Global Communications Conference Workshops [1].

Y. Oh, N. Lee, and Y.-S. Jeon are with the Department of Electrical Engineering, POSTECH, Pohang, Gyeongbuk 37673, South Korea (e-mails: {yongjeongoh,nylee,yoseb.jeon}@postech.ac.kr).

H. V. Poor is with the Department of Electrical and Computer Engineering, Princeton University, Princeton, NJ 08544 (e-mail: poor@princeton.edu).

## I. INTRODUCTION

Federated learning is a decentralized artificial intelligence (AI) technique for training a *global* model on a parameter server (PS) through collaboration with wireless devices, each with its own local training dataset [2]–[6]. The most widely adopted approach in federated learning is to update the global model by iterating the following two steps: (i) each wireless device updates a *local* model based on its local training dataset, then transmits the information of the local model update; (ii) the PS updates the global model by aggregating the local model updates transmitted by the devices, then broadcasts the updated model to the devices. Federated learning based on the above approach allows the PS to train the global model without direct access to the devices’ data and therefore can help preserve the privacy of the data generated at the devices. Thanks to this advantage, federated learning has received a great deal of attention as a means of enabling privacy-sensitive AI applications [4]–[9].

A major bottleneck in federated learning is significant communication overhead required when transmitting the local model updates from the wireless devices to the PS. This problem becomes more severe as the global model on the PS becomes more sophisticated, because the amount of the communication overhead increases with the number of global model parameters. To address this problem, gradient compression for federated learning is necessary, and several compression techniques have been intensively proposed in the literature [10]–[22]. The common idea of these techniques is to apply lossy compression to the local gradients of the model parameters computed at each device. Two representative approaches for gradient compression are *gradient quantization* and *gradient sparsification*. In the gradient quantization approach, local gradients are quantized and then transmitted using digital transmission [10]–[15]. A well-known technique based on this approach is one-bit quantization, in which the device only transmits the sign of each local gradient [12]. Vector quantization for gradient compression is also studied in [14], [15]. In these studies, the local gradients are partitioned into multiple groups; each group of the local gradients is quantized using vector quantizers such as lattice quantizers [14] and Grassmannian quantizers [15]. In the gradient sparsification approach, local gradients are sparsified by dropping less significant entries in their magnitudes. Analog transmission with gradient sparsification is studied in [21], [22] in which a local gradient vector after the sparsification is compressed by random projection onto a lower dimensional space as in compressed sensing (CS). Digital transmission with gradient sparsification is studied in [18]–[20] which an encoding function is

designed to exploit the sparsity of the local gradients.

Recently, gradient compression based on quantized compressed sensing (QCS) has been studied in [23]–[25] to take the advantages of both the gradient quantization and sparsification. A representative strategy towards this direction is gradient compression based on QCS with dithered uniform quantization [23]. A key advantage of this strategy is that quantization error can be transformed into an independent noise, which allows for the PS to reconstruct the local gradients using a simple linear estimator. This advantage, however, is attained at the cost of additional communication overhead because each device needs to additionally transmit its dither signal to the PS, which scales linearly with the number of global model parameters. Gradient compression based on QCS without dithered quantization is studied in [24], [25], in which binary iterative hard thresholding algorithm is adopted to reconstruct gradients at the PS. A common limitation of the strategies in [24], [25] is that they only operate with one-bit quantization and therefore suffer from high quantization error. Despite these efforts, none of the existing studies has developed gradient compression based on QCS with a multi-bit non-uniform scalar quantizer which has more flexibility to control the compression ratio and the quantization noise level than the existing work. More importantly, minimizing reconstruction error at the PS remains unsolved in federated learning with QCS-based gradient compression, which is essential to reduce the performance gap between centralized learning and federated learning.

In this paper, we present a communication-efficient federated learning framework, referred to as *FedQCS*. This framework consists of a gradient compression strategy for wireless devices and gradient reconstruction strategies for a PS. Our gradient compression strategy, inspired by QCS, effectively reduces communication overhead of transmitting a local gradient vector from each device to the PS, by taking the advantages of both the gradient quantization and sparsification. Meanwhile, our gradient reconstruction strategies enable accurate aggregation of the local gradients from the compressed signals at the PS. We also provide a convergence rate analysis of FedQCS. Using the MNIST dataset, we demonstrate that FedQCS with one bit overhead per gradient entry performs very close to the case with no compression, while outperforming the existing QCS-based federated learning frameworks. The major contributions of this paper are summarized as follows:

- We propose a gradient compression strategy to reduce communication overhead of transmitting a local gradient vector from each device to the PS. The key idea of our strategy is to sequentially perform (i) block sparsification, (ii) dimension reduction, and (iii) quantization.

In the block sparsification process, we divide the local gradient vector at each device into  $B$  sub-vectors, then sparsifies each sub-vector by dropping the least significant entries in their magnitudes. Then, in the dimension reduction process, we reduce the dimension of each sparsified sub-vector by applying random projection onto a lower dimensional space using a sensing matrix. Finally, in the quantization process, each entry of the low-dimensional sub-vector is quantized by using the optimal Lloyd-Max scalar quantizer. It is demonstrated that our compression strategy requires  $\frac{Q}{R}$  bits for conveying the information of each local gradient entry to the PS, where  $Q$  is the quantization bits of the scalar quantizer and  $R$  is a dimension reduction ratio. Therefore, our strategy not only provides a flexible communication overhead for federated learning, but also achieves a higher compression ratio than the state-of-the-art one-bit gradient compression (e.g., [12]) when  $Q < R$ .

- We develop two gradient reconstruction strategies for the PS, referred to as *estimate-and-aggregate* and *aggregate-and-estimate*, which enable accurate aggregation of local gradients from compressed signals. The key idea of the estimate-and-aggregate strategy is to first estimate each local gradient sub-vector from its compressed signal, then aggregate the estimated sub-vectors to reconstruct a global gradient vector. In this strategy, the problem of estimating each local gradient sub-vector is formulated as a *quantized* CS recovery problem. We solve this problem by employing a quantized variant of the expectation-maximization generalized-approximate-message-passing (EM-GAMP) algorithm in [26], [27] with Bernoulli Gaussian-mixture prior, which iteratively computes an approximate minimum mean square error (MMSE) estimate of the local gradient sub-vector from the compressed signal. Although the estimate-and-aggregate strategy approximately minimizes the MSE of the local gradient estimates, the computational complexity of this strategy increases linearly with the number of the devices. To mitigate this complexity requirement, in the aggregate-and-estimate strategy, we first aggregate the local gradient sub-vectors and then estimate the aggregated sub-vector. The underlying challenge in this strategy is that aggregation of the local gradient sub-vectors from the compressed signals is not straightforward due to nonlinearity of the quantization. To overcome this challenge, we use the Bussgang theorem in [28] to transform a nonlinear compressed signal into a linear compressed signal with additive distortion. Thanks to this theorem, the problem of estimating the aggregated sub-vector is formulated as an *unquantized but noisy* CS recovery problem. We solve this problem by employing the original EM-GAMP algorithm in [26], which iteratively computes an approximate MMSE

estimate of the aggregated sub-vector from its noisy linear observation. A key advantage of the aggregate-and-estimate strategy is that it can adjust the performance-complexity trade-off of the gradient reconstruction process by changing how many sub-vectors are aggregated before the estimation.

- We provide a convergence rate analysis of FedQCS using the aggregate-and-estimate strategy. To this end, we first characterize an MSE upper bound in reconstructing a global gradient vector based on the Bernoulli Gaussian-mixture modeling of the local gradient vector. Our analysis demonstrates that the reconstruction error reduces as a dimension reduction ratio,  $R$ , decreases and also as the number of the quantization bits,  $Q$ , increases. We then use the reconstruction error bound to characterize the convergence rate of FedQCS operating with a stochastic gradient descent (SGD) algorithm. From the analysis, we show that FedQCS is guaranteed to converge to a stationary point of a smooth loss function at the rate of  $\mathcal{O}(\frac{1}{\sqrt{T}})$ , where  $T$  is the number of total iterations of the SGD algorithm.
- Using simulations, we demonstrate the superiority of FedQCS over the existing QCS-based federated learning frameworks for an image classification task using the MNIST dataset [29]. Our simulation results demonstrate that FedQCS with one bit overhead per gradient entry suffices to attain the identical classification accuracy as perfect reconstruction with no compression. It is also shown that FedQCS outperforms the existing QCS-based frameworks in terms of both the classification accuracy and the normalized MSE of the gradient reconstruction. We also investigate the effect of the communication overhead, the dimension reduction ratio, the number of the quantization bits, and the sparsification level on the performance of FedQCS. From simulation results, we demonstrate that FedQCS effectively reduces communication overhead of federated learning while enabling accurate reconstruction of the global gradient vector at the PS.

*Notation:* Upper-case and lower-case boldface letters denote matrices and column vectors, respectively.  $\mathbb{E}[\cdot]$  is the statistical expectation, and  $(\cdot)^\top$  is the transpose.  $|\mathcal{A}|$  is the cardinality of set  $\mathcal{A}$ .  $(\mathbf{a})_i$  represents the  $i$ -th entry of vector  $\mathbf{a}$ .  $\|\mathbf{a}\| = \sqrt{\mathbf{a}^\top \mathbf{a}}$  is the Euclidean norm of a real vector  $\mathbf{a}$ .  $\mathcal{N}(\boldsymbol{\mu}, \mathbf{R})$  represents the distribution of a Gaussian random vector with mean vector  $\boldsymbol{\mu}$  and covariance matrix  $\mathbf{R}$ .  $\mathbf{0}_n$  is an  $n$ -dimensional vector with zero entries.  $\mathbf{I}_N$  is an  $N$  by  $N$  identity matrix.

## II. SYSTEM MODEL

We consider a federated learning scenario in which a global model on a parameter server (PS) is trained by collaborating with  $K$  wireless devices. A key assumption in federated learning is that data samples for training the global model are distributed over the wireless devices, while the PS has no direct access to these samples. We denote a set of training data samples available at device  $k \in \mathcal{K} = \{1, \dots, K\}$  by  $\mathcal{D}_k$ , which is hereafter referred to as a *local* training dataset. We also denote a parameter vector that represents the global model on the PS by  $\mathbf{w} \in \mathbb{R}^{\bar{N}}$ , where  $\bar{N}$  is the number of the parameters. For example, if the global model takes a form of a deep neural network (DNN), the entries of the parameter vector are the weights and the biases of the DNN. Then a *local* loss function at device  $k$  for the parameter vector  $\mathbf{w}$  is defined as

$$F_k(\mathbf{w}) = \frac{1}{|\mathcal{D}_k|} \sum_{\mathbf{u} \in \mathcal{D}_k} f(\mathbf{w}; \mathbf{u}), \quad (1)$$

where  $f(\mathbf{w}; \mathbf{u})$  is a loss function computed for the parameter vector  $\mathbf{w}$  with respect to a training data sample  $\mathbf{u} \in \mathcal{D}_k$ . Similarly, a *global* loss function for the parameter vector  $\mathbf{w}$  is defined as

$$F(\mathbf{w}) = \frac{1}{|\mathcal{D}|} \sum_{\mathbf{u} \in \mathcal{D}} f(\mathbf{w}; \mathbf{u}) = \frac{1}{\sum_{j=1}^K |\mathcal{D}_j|} \sum_{k=1}^K |\mathcal{D}_k| F_k(\mathbf{w}), \quad (2)$$

where  $\mathcal{D} = \cup_k \mathcal{D}_k$ . The ultimate goal of federated learning is to find the best parameter vector that minimizes the global loss function in (2). A practical solution to achieve this goal is to train the parameter vector based on a gradient-based optimizer such as a stochastic gradient descent algorithm and the ADAM optimizer in [30]. Let  $\mathbf{w}_t \in \mathbb{R}^{\bar{N}}$  be the parameter vector at iteration  $t \in \{1, \dots, T\}$  of the optimizer, where  $T$  is the total number of iterations. Then minimizing the loss function in (2) using the gradient-based optimizer requires the knowledge of a *true* gradient vector at the PS, defined as

$$\nabla F(\mathbf{w}_t) = \frac{1}{|\mathcal{D}|} \sum_{\mathbf{u} \in \mathcal{D}} \nabla f(\mathbf{w}_t; \mathbf{u}), \quad \forall t \in \{1, \dots, T\}. \quad (3)$$

In federated learning, training data samples are available only at the wireless devices; thereby, the true gradient vector in (3) cannot be computed at the PS directly. As an alternative solution, the PS acquires the knowledge of the gradient vector by collaborating with the wireless devices as described below.

**Operations at the wireless devices:** Suppose that all the wireless devices have the information of a globally consistent parameter vector  $\mathbf{w}_t$ . Each wireless device computes a *local* gradient

vector based on its own local training dataset. A local gradient vector computed at device  $k$  for the parameter vector  $\mathbf{w}_t$  is given by

$$\nabla F_k^{(t)}(\mathbf{w}_t) = \frac{1}{|\mathcal{D}_k^{(t)}|} \sum_{\mathbf{u} \in \mathcal{D}_k^{(t)}} \nabla f(\mathbf{w}_t; \mathbf{u}), \quad (4)$$

where  $\nabla$  is a gradient operator, and  $\mathcal{D}_k^{(t)} \subset \mathcal{D}_k$  is a mini-batch randomly drawn from  $\mathcal{D}_k$  at iteration  $t$ . Then all the devices send the information of their local gradient vectors to the PS. Since direct transmission of the local gradient vector in (4) imposes large communication overhead when  $\bar{N} \gg 1$ , we assume that each device applies *lossy* compression to its local gradient vector before the transmission. Our strategy for compressing the local gradient vectors will be described in Sec. III.

**Operations at the parameter server:** Based on compressed local gradient vectors sent by the wireless devices, the PS attempts to reconstruct a *global* gradient vector defined as

$$\mathbf{g}_{\mathcal{K}}^{(t)} = \sum_{k=1}^K \rho_k^{(t)} \nabla F_k^{(t)}(\mathbf{w}_t), \quad (5)$$

where  $\rho_k^{(t)} \triangleq \frac{|\mathcal{D}_k^{(t)}|}{\sum_{j=1}^K |\mathcal{D}_j^{(t)}|}$ . Since the lossy compression is applied at the wireless devices, perfect reconstruction of the global gradient vector is not feasible at the PS. As a result, a global gradient vector reconstructed at the PS, namely  $\hat{\mathbf{g}}_{\mathcal{K}}^{(t)} \in \mathbb{R}^{\bar{N}}$ , contains reconstruction error. Our strategy to minimize this error will be elucidated in Sec. IV. After the gradient reconstruction, the PS updates the parameter vector according to the optimizer based on the information of  $\hat{\mathbf{g}}_{\mathcal{K}}^{(t)}$ . For example, if a gradient descent algorithm is employed at the PS, the corresponding update rule is given by

$$\mathbf{w}_{t+1} \leftarrow \mathbf{w}_t - \eta_t \hat{\mathbf{g}}_{\mathcal{K}}^{(t)}, \quad (6)$$

where  $\eta_t > 0$  is a learning rate at iteration  $t$ . Finally, the PS broadcasts the updated parameter vector to the wireless devices.

The federated learning scenario described above is illustrated in Fig. 1. Under this scenario, the major contribution of this work is to present a novel federated learning framework by developing (i) a local gradient compression strategy for the wireless devices and (ii) global gradient reconstruction strategies for the PS. We refer to this framework as federated learning via quantized compressed sensing (FedQCS).

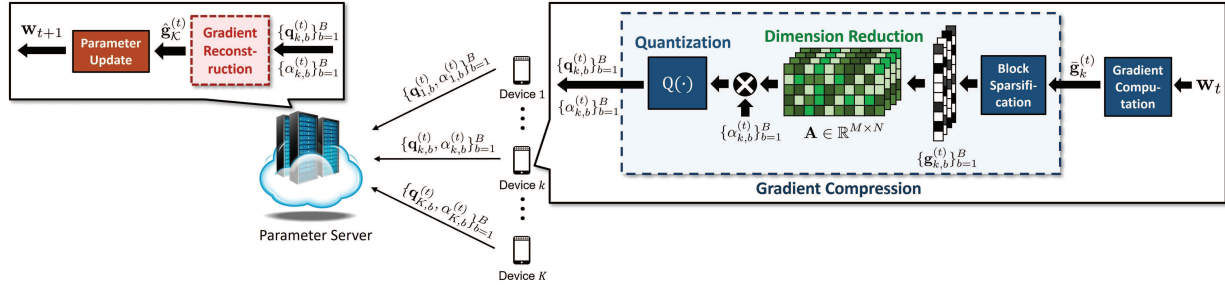


Fig. 1. An illustration of the proposed federated learning framework.

### III. GRADIENT COMPRESSION STRATEGY OF FEDQCS

Communication overhead reduction in federated learning is essential when optimizing the loss function with a very large model size such as DNNs. In this section, we propose a lossy gradient compression strategy which effectively reduces the communication overhead required when transmitting a local gradient vector from each device to the PS.

#### A. Proposed Compression Strategy

The key idea of the proposed strategy, inspired by QCS, is to sequentially perform (i) block sparsification, (ii) dimension reduction, and (iii) quantization. We refer to this strategy as *BQCS* compression as it performs block sparsification before applying the compression based on QCS. The overall procedure of the BQCS compression is summarized in Steps 4–8 in **Procedure 1**, while details of each process are elaborated below.

**Block Sparsification:** In the block sparsification process, each device divides its gradient vector into  $B$  sub-vectors, each of which has a dimension of  $N = \frac{\bar{N}}{B}$ , then sparsifies each sub-vector by dropping the least significant entries in terms of their magnitudes. Let  $\bar{g}_k^{(t)} \in \mathbb{R}^N$  be a *target* local gradient vector computed by device  $k$  at iteration  $t$ . Also, let  $\mathcal{N}_1, \dots, \mathcal{N}_B$  be mutually exclusive subsets of  $\bar{\mathcal{N}} = \{1, \dots, \bar{N}\}$  such that  $\bigcup_{b=1}^B \mathcal{N}_b = \bar{\mathcal{N}}$ . Then the  $b$ -th local gradient sub-vector at device  $k$  is defined as  $\bar{g}_{k,b}^{(t)} = [\bar{g}_{k,\mathcal{N}_b(1)}^{(t)}, \dots, \bar{g}_{k,\mathcal{N}_b(N)}^{(t)}]^\top$ , where  $\bar{g}_{k,i}^{(t)}$  is the  $i$ -th entry of  $\bar{g}_k^{(t)}$ . Then an  $S$ -sparse vector  $g_{k,b}^{(t)} \in \mathbb{R}^N$  is generated from  $\bar{g}_{k,b}^{(t)}$  by dropping all but the top- $S$  entries with the largest magnitudes. For ease of exposition, we denote the block sparsification process applied to the local gradient vector  $\bar{g}_k^{(t)}$  as  $\text{BlockSparse}(\bar{g}_k^{(t)})$  whose output is given by  $\{g_{k,b}^{(t)}\}_{b=1}^B$ . One drawback of the block sparsification process is that gradient information is lost when dropping the least significant gradient entries. Fortunately, this information loss can be partially compensated by accumulating the dropped gradient entries and then by adding these



entries in the next iteration [21], [22]. Motivated by this fact, the block sparsification process is performed in conjunction with gradient accumulation as follows: Let  $\Delta_k^{(t)} \in \mathbb{R}^{\bar{N}}$  be a residual gradient vector of device  $k$  at iteration  $t + 1$ , defined as

$$\Delta_k^{(t+1)} = \bar{\mathbf{g}}_k^{(t)} - \text{Concatenate}(\{\mathbf{g}_{k,b}^{(t)}\}_{b=1}^B), \quad (7)$$

where  $\text{Concatenate}(\{\mathbf{g}_{k,b}^{(t)}\}_{b=1}^B)$  is a function that concatenates  $B$  sub-vectors  $\{\mathbf{g}_{k,b}^{(t)}\}_{b=1}^B$  into the form of the original vector  $\mathbf{g}_k^{(t)}$ . The residual vector  $\Delta_k^{(t+1)}$  is stored at device  $k$  and then added to the next local gradient vector at iteration  $t + 1$ :

$$\bar{\mathbf{g}}_k^{(t+1)} = \nabla F_k^{(t+1)}(\mathbf{w}_{t+1}) + \Delta_k^{(t+1)}. \quad (8)$$

The local gradient vector in (8) is applied as the input of the block sparsification process at iteration  $t + 1$ .

**Dimension Reduction:** In the dimension reduction process, each gradient sub-vector is projected onto a lower dimensional space using a sensing matrix  $\mathbf{A} \in \mathbb{R}^{M \times N}$  with  $M < N$ . Then a low-dimensional projection of a gradient sub-vector  $\mathbf{g}_{k,b}^{(t)}$  is represented as

$$\mathbf{x}_{k,b}^{(t)} = \alpha_{k,b}^{(t)} \mathbf{A} \mathbf{g}_{k,b}^{(t)}, \quad (9)$$

where  $\alpha_{k,b}^{(t)}$  is a scaling factor. In this process, the choice of the sensing matrix  $\mathbf{A}$  is critical to successful recovery of local gradients at the PS. In CS theory, it is shown that if  $\mathbf{A}$  is an independent and identically distributed (IID) random matrix with  $(\mathbf{A})_{m,n} \sim \mathcal{N}(0, 1/M)$  for  $M = \mathcal{O}(S \log(N/S)/\delta_{2S}^2)$ , there exists  $\delta_{2S} \in (0, 1)$  such that  $(1 - \delta_{2S})\|\mathbf{g}\|^2 \leq \|\mathbf{A}\mathbf{g}\|^2 \leq (1 + \delta_{2S})\|\mathbf{g}\|^2$  with high probability, which is called the restricted isometry property (RIP) of order  $2S$  [31]. This condition is known to be sufficient for a variety of algorithms to enable successful recovery of a sparse signal from noisy linear measurements [31]. Motivated by this fact, we set  $\mathbf{A}$  as an IID random matrix with  $(\mathbf{A})_{m,n} \sim \mathcal{N}(0, 1/M)$ . Under this choice, it is expected that  $\mathbb{E}[\|\mathbf{x}_{k,b}^{(t)}\|^2] = (\alpha_{k,b}^{(t)})^2 \|\mathbf{g}_{k,b}^{(t)}\|^2$ . Based on this fact, we also set the scaling factor as  $\alpha_{k,b}^{(t)} = \sqrt{M}/\|\mathbf{g}_{k,b}^{(t)}\|$  which guarantees that every low-dimensional sub-vector has an equal power of  $M$ , for all  $k, b, t$ . This property will be utilized in the design of a scalar quantizer in the subsequent quantization process.

**Quantization:** In the quantization process, each entry of a low-dimensional sub-vector is quantized by using a  $Q$ -bit scalar quantizer. Let  $\mathcal{Q} : \mathbb{R} \rightarrow \mathcal{Q} \triangleq \{q_1, \dots, q_{2^Q}\}$  be a  $Q$ -bit scalar quantizer that maps a real value input to the nearest point in  $\mathcal{Q}$ , i.e.,  $\mathcal{Q}(x) = q_i$  if  $x \in (\tau_{i-1}, \tau_i]$ ,

where  $q_i$  is the  $i$ -th quantizer output, and  $\tau_i$  is the  $i$ -th quantizer threshold with  $\tau_0 < \dots < \tau_{2Q}$  with  $\tau_0 = -\infty$  and  $\tau_{2Q} = \infty$ . Then the quantized sub-vector at device  $k$  is obtained as

$$\mathbf{q}_{k,b}^{(t)} = \mathbf{Q}(\mathbf{x}_{k,b}^{(t)}). \quad (10)$$

Since the accuracy of gradient reconstruction at the PS is closely related to a quantization error, given by  $\mathbf{Q}(\mathbf{x}_{k,b}^{(t)}) - \mathbf{x}_{k,b}^{(t)}$ , we also optimize the design of the scalar quantizer to minimize the MSE of the quantizer output by leveraging the Lloyd-Max algorithm [32]. To this end, the knowledge of the distribution of  $\mathbf{x}_{k,b}^{(t)}$  is required at the devices, which is challenging in federated learning due to the difficulty in characterizing the distribution of local gradients. To circumvent this challenge, instead of characterizing the exact distribution, we model each local gradient sub-vector as an IID random vector by using an approximate distribution (e.g., a Bernoulli Gaussian-mixture distribution), as will be justified in Sec. IV-A. Under this approximate model, the projection in (9) with  $(\mathbf{A})_{m,n} \sim \mathcal{N}(0, 1/M)$  implies that each entry of  $\mathbf{x}_{k,b}^{(t)}$  behaves like a zero-mean Gaussian random variable for large  $N$  by the central limit theorem. Meanwhile, the choice of  $\alpha_{k,b}^{(t)} = \sqrt{M}/\|\mathbf{g}_{k,b}^{(t)}\|$  implies that  $\mathbb{E}[\|\mathbf{x}_{k,b}^{(t)}\|^2] = M$ . Therefore, every entry of  $\mathbf{x}_{k,b}^{(t)}$  can be effectively modeled by a Gaussian random variable with zero mean and unit variance. Motivated by this fact, we employ the Lloyd-Max scalar quantizer optimized for the distribution of  $\mathcal{N}(0, 1)$ . A key benefit of our optimization is that the design of the scalar quantizer does not depend on the indexes  $k, b, t$ ; thereby, the optimal scalar quantizer can be shared by all the devices and the PS in prior without explicit information exchange.

### B. Communication Overhead of BQCS Compression

When employing the proposed BQCS compression, each device  $k$  needs to convey the information of  $\{\mathbf{q}_{k,b}^{(t)}, \alpha_{k,b}^{(t)}\}_{b=1}^B$  to the PS. Note that  $Q$  bits are required to transmit each entry of  $\mathbf{q}_{k,b}^{(t)}$ , while 32 bits are required to transmit  $\alpha_{k,b}^{(t)}$  using floating-point representation. Since 32-bit overhead is negligible compared to  $QM$  bits, communication overhead of the proposed compression becomes  $\frac{QMB}{NB} = \frac{Q}{R}$  bits per gradient entry, where  $R \triangleq \frac{N}{M} > 1$  is a dimension reduction ratio. This fact clearly reveals that the communication overhead of the BQCS compression is adjustable by changing the number of quantization bits,  $Q$ , and the dimension reduction ratio,  $R$ . A more important observation is that by choosing  $Q < R$ , the communication overhead of our compression can be made even less than one bit per gradient entry. Thanks to this feature, our strategy achieves a higher compression ratio than the state-of-the-art one-bit gradient

---

**Procedure 1** Federated Learning via Quantized Compressed Sensing (FedQCS)

---

**Input:** Initial parameter vector  $\mathbf{w}_1$ ,  $\Delta_k^{(1)} = \mathbf{0}_{\bar{N}}$ ,  $\{\mathcal{N}_b\}_{b=1}^B$ ,  $\{\mathcal{K}_g\}_{g=1}^G$

**Output:** Optimized parameter vector  $\mathbf{w}_T$

- 1: **for**  $t = 1$  to  $T$  **do**
  - 2:   *At the wireless devices:*
  - 3:   **for** Each device  $k \in \mathcal{K}$  **do**
  - 4:      $\bar{\mathbf{g}}_k^{(t)} = \nabla F_k^{(t)}(\mathbf{w}_t) + \Delta_k^{(t)}$ .
  - 5:      $\{\mathbf{g}_{k,b}^{(t)}\}_{b=1}^B = \text{BlockSparse}(\bar{\mathbf{g}}_k^{(t)})$ .
  - 6:      $\Delta_k^{(t+1)} = \bar{\mathbf{g}}_k^{(t)} - \text{Concatenate}(\{\mathbf{g}_{k,b}^{(t)}\}_{b=1}^B)$ .
  - 7:      $\mathbf{q}_{k,b}^{(t)} = \mathbf{Q}(\mathbf{x}_{k,b}^{(t)})$  where  $\mathbf{x}_{k,b}^{(t)} = \alpha_{k,b}^{(t)} \mathbf{A} \mathbf{g}_{k,b}^{(t)}$ ,  $\forall b$ .
  - 8:     Push  $\{\mathbf{q}_{k,b}^{(t)}, \alpha_{k,b}^{(t)}\}_{b=1}^B$  to the parameter server.
  - 9:   **end for**
  - 10:   *At the parameter server:*
  - 11:   **if** Estimate-and-aggregate strategy **then**
  - 12:      $\hat{\mathbf{g}}_{k,b}^{(t)} = \text{QEMGAMP}(\mathbf{q}_{k,b}^{(t)}, \alpha_{k,b}^{(t)}, \mathbf{A})$  from **Procedure 2**,  $\forall k, b$ .
  - 13:      $\hat{\mathbf{g}}_k^{(t)} = \text{Concatenate}(\{\hat{\mathbf{g}}_{k,b}^{(t)}\}_{b=1}^B)$ ,  $\forall k$ .
  - 14:      $\hat{\mathbf{g}}_{\mathcal{K}}^{(t)} = \sum_{k=1}^K \rho_k^{(t)} \hat{\mathbf{g}}_k^{(t)}$ .
  - 15:   **else if** Aggregate-and-estimate strategy **then**
  - 16:      $\tilde{\mathbf{q}}_{\mathcal{K}_g,b}^{(t)} = \sum_{k \in \mathcal{K}_g} \{\rho_k^{(t)} / (\gamma_Q \alpha_{k,b}^{(t)})\} \mathbf{q}_{k,b}^{(t)}$ ,  $\forall g, b$ .
  - 17:      $\nu_{g,b}^{(t)} = (\psi_Q - \gamma_Q^2) / \gamma_Q^2 \sum_{k \in \mathcal{K}_g} \{\rho_k^{(t)} / \alpha_{k,b}^{(t)}\}^2$ ,  $\forall g, b$ .
  - 18:      $\hat{\mathbf{g}}_{\mathcal{K}_g,b}^{(t)} = \text{EMGAMP}(\tilde{\mathbf{q}}_{\mathcal{K}_g,b}^{(t)}, \nu_{g,b}^{(t)}, \mathbf{A})$ ,  $\forall g, b$ .
  - 19:      $\hat{\mathbf{g}}_{\mathcal{K}_g}^{(t)} = \text{Concatenate}(\{\hat{\mathbf{g}}_{\mathcal{K}_g,b}^{(t)}\}_{b=1}^B)$ ,  $\forall g$ .
  - 20:      $\hat{\mathbf{g}}_{\mathcal{K}}^{(t)} = \sum_{g=1}^G \hat{\mathbf{g}}_{\mathcal{K}_g}^{(t)}$ .
  - 21:   **end if**
  - 22:    $\mathbf{w}_{t+1} = \mathbf{w}_t - \eta_t \hat{\mathbf{g}}_{\mathcal{K}}^{(t)}$ .
  - 23:   Broadcast  $\mathbf{w}_{t+1}$  to the wireless devices.
  - 24: **end for**
- 

compression [12]. In Sec. VI, we will also demonstrate that the BQCS compression enables more accurate reconstruction of the global gradient vector at the PS compared to the one-bit gradient compression.

**Remark 1 (Comparison to Existing QCS-based Gradient Compression):** We highlight the major differences between the BQCS compression and the existing QCS-based gradient compression methods in [23]–[25]. The compression method in [23] adopts dithered uniform

quantization combined with dimension reduction. A key advantage of the dithered quantization is that the quantized signal can be transformed into the sum of a quantizer input signal and an independent quantization noise when the uniform quantizer is adopted with random dither signals [33]. This advantage, however, is attained at the cost of additional communication overhead because the information of the dither signal (with dimension  $\bar{N}$ ) should be separately conveyed to the PS for gradient reconstruction. In addition, the use of the uniform quantizer leads to larger quantization error compared to the optimal quantizer used in our BQCS compression. The compression method in [24], [25] adopts one-bit scalar quantization combined with dimension reduction, which is also known as one-bit compressed sensing. In this method, the number of quantization bits is fixed to only one (i.e.,  $Q = 1$ ); thereby, communication overhead of this method is less flexible than that of the BSDQ compression. In Sec. VI, we will also demonstrate that our BQCS compression enables more accurate gradient reconstruction at the PS compared to the existing compression methods under the same communication overhead.

#### IV. GRADIENT RECONSTRUCTION STRATEGIES OF FEDQCS

One of the primary goals at the PS is to accurately reconstruct the global gradient vector in (5) from the local gradient vectors sent by wireless devices, in order to optimize the parameter vector  $\mathbf{w}$ . Unfortunately, the use of the BQCS compression in Sec. III brings a new challenge in realizing accurate gradient reconstruction at the PS because the local gradient vectors sent by the device are not only projected onto a low-dimensional space as done in CS, but also nonlinearly distorted by scalar quantization. In this section, we tackle this challenge by presenting two gradient reconstruction strategies, referred to as *estimate-and-aggregate* and *aggregate-and-estimate*, which enable accurate aggregation of the local gradients from the compressed signals.

##### A. Estimate-and-Aggregate Strategy

The key idea of the estimate-and-aggregate strategy is to first estimate each local gradient sub-vector from its compressed signal, then aggregate the estimated sub-vector to reconstruct a global gradient vector. In this strategy, the problem of estimating a local gradient sub-vector,  $\mathbf{g}_{k,b}^{(t)}$ , from its compressed signal,  $\mathbf{q}_{k,b}^{(t)} = \mathbf{Q}(\alpha_{k,b}^{(t)} \mathbf{A} \mathbf{g}_{k,b}^{(t)})$ , is nothing but a QCS recovery problem. There are two underlying challenges to solve this problem: (i) finding the optimal solution of a QCS recovery problem in terms of minimizing the reconstruction error is still an open problem [27], [34], and (ii) the distribution of the local gradient sub-vectors is generally unknown at the

PS which prevents the PS from directly applying a Bayesian inference approach. To circumvent these challenges, we employ a quantized EM-GAMP (Q-EM-GAMP) algorithm in [27] which iteratively computes an *approximate* MMSE solution of a QCS recovery problem while learning the distribution of an unknown signal via the EM principle.

To employ the Q-EM-GAMP algorithm to solve our QCS recovery problem, each local gradient sub-vector needs to be modeled as an IID random vector with a proper distribution. Inspired by the sparse property as well as the arbitrary random nature of the local gradient sub-vector, we model each sub-vector using a Bernoulli Gaussian-mixture distribution which is well known for its suitability and generality for modeling a sparse random vector [26], [27]. Note that the probability density function of the Bernoulli Gaussian-mixture distribution with parameter  $\boldsymbol{\theta} = (\lambda_0, \{\lambda_l, \mu_l, \phi_l\}_{l=1}^L)$  is given by

$$\mathcal{BG}(g; \boldsymbol{\theta}) = \lambda_0 \delta(g) + \sum_{l=1}^L \frac{\lambda_l}{\sqrt{2\pi\phi_l}} \exp\left(-\frac{(g - \mu_l)^2}{2\phi_l}\right). \quad (11)$$

As can be seen in (11), the sparse property of the local gradient sub-vector is captured by the Bernoulli distribution with parameter  $\lambda_0$ . Meanwhile, the arbitrary random nature of non-zero entries can be effectively approximated by a Gaussian-mixture distribution with  $L$  components, where the mean and the variance of the  $l$ -th component are denoted by  $\mu_l$  and  $\phi_l$ , respectively. Assuming IID Bernoulli Gaussian-mixture prior, the Q-EM-GAMP algorithm computes an approximate MMSE estimate of  $\mathbf{g}_{k,b}^{(t)}$  from  $\mathbf{q}_{k,b}^{(t)}$  by iterating the following two steps: (i) perform the GAMP algorithm to compute the approximate MMSE estimate of  $\mathbf{g}_{k,b}^{(t)}$  from  $\mathbf{q}_{k,b}^{(t)}$  by assuming that each entry of  $\mathbf{g}_{k,b}^{(t)}$  follows the Bernoulli Gaussian-mixture prior with parameter  $\boldsymbol{\theta}_{k,b}^{(t)}$ ; (ii) update the parameter  $\boldsymbol{\theta}_{k,b}^{(t)}$  of the Bernoulli Gaussian-mixture model based on the EM principle. The Q-EM-GAMP algorithm utilized in our parallel recovery strategy is summarized in **Procedure 2**, where we omit the indexes  $k$ ,  $b$ , and  $t$ , for the sake of brevity.

The major steps in **Procedure 2** are elaborated below. In Steps 5 and 6, the prior mean  $\hat{p}_m$  and variance  $\nu_{p_m}$  of  $x_m$  are estimated. In Steps 7 and 8, the posterior mean and variance of  $x_m$  are computed under the assumption of  $x_m \sim \mathcal{N}(\hat{p}_m, \nu_{p_m})$ , given by

$$\hat{x}_m^{\text{post}} = \int_{-\infty}^{\infty} x_m p(x_m | q_m) dx_m = \hat{p}_m + \nu_{p_m} \frac{p'(q_m)}{p(q_m)}, \quad (12)$$

$$\nu_{x_m}^{\text{post}} = \int_{-\infty}^{\infty} x_m^2 p(x_m | q_m) dx_m - (\hat{x}_m^{\text{post}})^2 = \nu_{p_m}^2 \left\{ \frac{p''(q_m)}{p(q_m)} - \left( \frac{p'(q_m)}{p(q_m)} \right)^2 \right\} + \nu_{p_m}, \quad (13)$$

---

**Procedure 2** The Q-EM-GAMP Algorithm
 

---

**Input:**  $\mathbf{q} \in \mathcal{Q}^M$ ,  $\alpha \in \mathbb{R}$ ,  $\mathbf{A} \in \mathbb{R}^{M \times N}$ 
**Output:**  $\hat{\mathbf{g}} \in \mathbb{R}^N$ 

- 1: Initialize  $\hat{g}_n \sim \mathcal{N}(0, \frac{M}{N\alpha^2})$ ,  $\nu_{g_n} = \frac{M}{N\alpha^2}$ , and  $\boldsymbol{\theta} = (\lambda_0, \{\lambda_l, \mu_l, \phi_l\}_{l=1}^L)$ .
  - 2: Set  $\hat{s}_m = 0$  and  $\tilde{a}_{m,n} = \alpha(\mathbf{A})_{m,n}$ ,  $\forall m, n$ .
  - 3: **for**  $i = 1$  to  $I_{\text{GAMP}}$  **do**
  - 4:    $\hat{g}_n^{\text{old}} = \hat{g}_n$ ,  $\forall n$ .
  - 5:    $\nu_{p_m} = \sum_{n=1}^N |\tilde{a}_{m,n}|^2 \nu_{g_n}$ ,  $\forall m$ .
  - 6:    $\hat{p}_m = \sum_{n=1}^N \tilde{a}_{m,n} \hat{g}_n - \nu_{p_m} \hat{s}_m$ ,  $\forall m$ .
  - 7:    $\hat{x}_m^{\text{post}} = \mathbb{E}[x_m | q_m, \hat{p}_m, \nu_{p_m}]$  from (12),  $\forall m$ .
  - 8:    $\nu_{x_m}^{\text{post}} = \text{Var}[x_m | q_m, \hat{p}_m, \nu_{p_m}]$  from (13),  $\forall m$ .
  - 9:    $\hat{s}_m = (\hat{x}_m^{\text{post}} - \hat{p}_m) / \nu_{p_m}$ ,  $\forall m$ .
  - 10:    $\nu_{s_m} = (1 - \nu_{x_m}^{\text{post}} / \nu_{p_m}) / \nu_{p_m}$ ,  $\forall m$ .
  - 11:    $\hat{r}_n = \hat{g}_n + \nu_{r_n} \sum_{m=1}^M \tilde{a}_{m,n} \hat{s}_m$ ,  $\forall n$ .
  - 12:    $\nu_{r_n} = (\sum_{m=1}^M |\tilde{a}_{m,n}|^2 \nu_{s_m})^{-1}$ ,  $\forall n$ .
  - 13:    $\hat{g}_n = \sum_{l=1}^L \lambda'_{n,l} \mu'_{n,l}$ ,  $\forall n$ .
  - 14:    $\nu_{g_n} = \sum_{l=1}^L \lambda'_{n,l} (\phi'_{n,l} + (\mu'_{n,l})^2) - (\hat{g}_n)^2$ ,  $\forall n$ .
  - 15:    $\boldsymbol{\theta} \leftarrow (\lambda''_0, \{\lambda''_l, \mu''_l, \phi''_l\}_{l=1}^L)$  from (17).
  - 16:   Break if  $\sum_{n=1}^N (\hat{g}_n^{\text{old}} - \hat{g}_n)^2 < \tau_{\text{GAMP}} \sum_{n=1}^N (\hat{g}_n^{\text{old}})^2$ .
  - 17: **end for**
  - 18:  $\hat{\mathbf{g}} = [\hat{g}_1, \dots, \hat{g}_N]^T$ .
- 

where

$$p(q_m) = Q\left(\frac{\tau_{i-1} - \hat{p}_m}{\sqrt{\nu_{p_m}}}\right) - Q\left(\frac{\tau_i - \hat{p}_m}{\sqrt{\nu_{p_m}}}\right), \quad (14)$$

$$p'(q_m) = \frac{1}{\sqrt{\nu_{p_m}}} \left[ \phi\left(\frac{\tau_{i-1} - \hat{p}_m}{\sqrt{\nu_{p_m}}}\right) - \phi\left(\frac{\tau_i - \hat{p}_m}{\sqrt{\nu_{p_m}}}\right) \right], \quad (15)$$

$$p''(q_m) = \frac{1}{\nu_{p_m}} \left[ \phi\left(\frac{\tau_{i-1} - \hat{p}_m}{\sqrt{\nu_{p_m}}}\right) \left(\frac{\tau_{i-1} - \hat{p}_m}{\sqrt{\nu_{p_m}}}\right) - \phi\left(\frac{\tau_i - \hat{p}_m}{\sqrt{\nu_{p_m}}}\right) \left(\frac{\tau_i - \hat{p}_m}{\sqrt{\nu_{p_m}}}\right) \right], \quad (16)$$

with  $Q(x) = \int_x^\infty \frac{1}{\sqrt{2\pi}} e^{-\frac{u^2}{2}} du$  and  $\phi(x) = \frac{1}{\sqrt{2\pi}} e^{-\frac{x^2}{2}}$ . In Steps 11 and 12,  $\hat{r}_n$  represents the observation of  $g_n$  under zero-mean Gaussian noise, while  $\nu_{r_n}$  represents the variance of the noise. In Steps 13 and 14, the posterior mean and variance of  $g_n$  are computed under the assumptions of  $g_n \sim \mathcal{BG}(\boldsymbol{\theta})$  and  $\hat{r}_n = g_n + \xi_n$  with  $\xi \sim \mathcal{N}(0, \nu_{r_n})$  as derived in [26], where  $\beta_{n,0} = \lambda_0 \mathcal{N}(0; \hat{r}_n, \nu_{r_n})$ ,  $\beta_{n,l} = \lambda_l \mathcal{N}(\hat{r}_n; \mu_l, \nu_{r_n} + \phi_l)$ ,  $\lambda'_{n,0} = \beta_{n,0} / (\beta_{n,0} + \sum_{i=1}^L \beta_{n,i})$ ,  $\lambda'_{n,l} = \beta_{n,l} / (\beta_{n,0} + \sum_{i=1}^L \beta_{n,i})$ ,

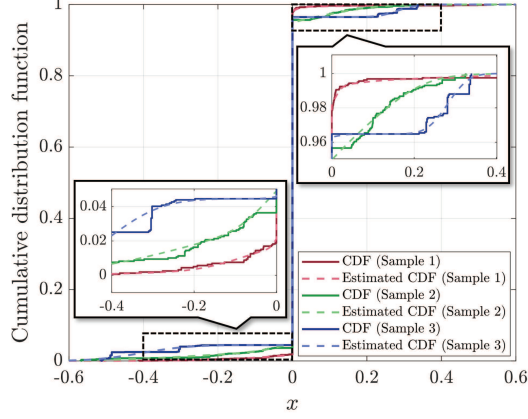


Fig. 2. Comparison between the empirical CDF of a local gradient sub-vector and an estimated CDF using a Bernoulli Gaussian-mixture distribution.

$\mu'_{n,l} = (\hat{r}_n \phi_l + \mu_l \nu_{r_n}) / (\nu_{r_n} + \phi_l)$ ,  $\phi'_{n,l} = \nu_{r_n} \phi_l / (\nu_{r_n} + \phi_l)$ , and  $\mathcal{N}(x; \mu_x, \nu_x) = \frac{1}{\sqrt{2\pi\nu_x}} e^{-\frac{(x-\mu_x)^2}{2\nu_x}}$ .

In Step 15, the parameters of the Bernoulli Gaussian-mixture model in (11) are computed based on the EM principle as derived in [26], where  $\lambda''_0 = \frac{1}{N} \sum_{n=1}^N \lambda'_{n,0}$ ,

$$\lambda''_l \approx \frac{1}{N} \sum_{n=1}^N \lambda'_{n,l}, \quad \mu''_l \approx \frac{\sum_{n=1}^N \lambda'_{n,l} \mu'_{n,l}}{\sum_{n=1}^N \lambda'_{n,l}}, \quad \phi''_{n,l} \approx \frac{\sum_{n=1}^N \lambda'_{n,l} \{(\mu_l - \mu'_{n,l})^2 + \phi'_{n,l}\}}{\sum_{n=1}^N \lambda'_{n,l}}, \quad (17)$$

for  $l \in \{1, \dots, L\}$ .

After computing the estimates of the local gradient sub-vectors, we aggregate these estimates to reconstruct the global gradient vector in (5). Let  $\hat{\mathbf{g}}_{k,b}^{(t)}$  be the estimate of  $\mathbf{g}_{k,b}^{(t)}$  computed by applying the Q-EM-GAMP algorithm to  $\mathbf{q}_{k,b}^{(t)}$ . Then the global gradient vector  $\hat{\mathbf{g}}_{\mathcal{K}}^{(t)}$  is obtained as

$$\hat{\mathbf{g}}_{\mathcal{K}}^{(t)} = \sum_{k=1}^K \rho_k^{(t)} \hat{\mathbf{g}}_k^{(t)}, \quad (18)$$

where  $\hat{\mathbf{g}}_k^{(t)} = \text{Concatenate}(\{\hat{\mathbf{g}}_{k,b}^{(t)}\}_{b=1}^B)$ . The overall gradient reconstruction process of our estimate-and-aggregate strategy is summarized in Steps 12–14 of **Procedure 1**.

**Validation for IID Bernoulli Gaussian-mixture prior:** We verify the tightness of the statistical model utilized in the Q-EM-GAMP algorithm using a simple numerical example. In this example, we consider an image classification task using the MNIST dataset when  $(R, Q) = (3, 3)$  and  $T = 1$ . Further details of the simulation are described in Sec. VI. Fig. 2 compares the *empirical* cumulative distribution function (CDF) of the local gradient entries sampled from simulation with the CDF of the Bernoulli Gaussian-mixture distribution whose parameters are determined by **Procedure 2**. Samples 1, 2, and 3 in Fig. 2 correspond to the gradient sub-vectors sampled when  $(k, b) = (1, 1)$ ,  $(15, 5)$ , and  $(30, 10)$ , respectively. Our numerical example

demonstrates that the empirical CDF of the local gradient sub-vectors are almost the same with the estimated CDF obtained based on our statistical model. This result implies that the local gradient sub-vector is effectively modeled as an IID random vector with the Bernoulli Gaussian-mixture distribution.

### B. Aggregate-and-Estimate Strategy

Although the estimate-and-aggregate strategy in Sec. IV-A has a potential to minimize the MSE of local gradient estimates at the PS, the computational complexity of this strategy increases linearly with the number of wireless devices as the PS needs to perform the Q-EM-GAMP algorithm  $KB$  times to reconstruct the global gradient vector in (5). To mitigate this complexity requirement, we develop an aggregate-and-estimate strategy which promotes more flexibility on the complexity of the gradient reconstruction process.

The key idea of the aggregate-and-estimate strategy is to first aggregate a group of local gradient sub-vectors, then estimate the aggregated sub-vector. In particular, we randomly divide  $K$  devices into  $G$  groups, then estimate an aggregated sub-vector for each group, defined as

$$\mathbf{g}_{\mathcal{K}_g,b}^{(t)} = \sum_{k \in \mathcal{K}_g} \rho_k^{(t)} \mathbf{g}_{k,b}^{(t)}, \quad \forall g \in \{1, \dots, G\}, \quad (19)$$

where  $\mathcal{K}_g$  is the index set of the devices in the  $g$ -th group, and  $\mathcal{K}_1, \dots, \mathcal{K}_G$  are mutually exclusive subsets of  $\mathcal{K}$  such that  $\mathcal{K} = \bigcup_{g=1}^G \mathcal{K}_g$ . The underlying difficulty in this strategy is that aggregating the local gradient sub-vectors,  $\{\mathbf{g}_{k,b}^{(t)}\}_{k \in \mathcal{K}_g}$ , from the quantized sub-vectors,  $\{\mathbf{q}_{k,b}^{(t)}\}_{k \in \mathcal{K}_g}$ , is not straightforward due to nonlinearity of scalar quantization. To tackle this difficulty, we use the Bussgang theorem in [28] which provides a theoretical basis to transform a quantization of a Gaussian signal into a linear signal with additive distortion. Recall that each entry of  $\mathbf{x}_{k,b}^{(t)}$  behaves like a Gaussian random variable with zero mean and unit variance for large  $N$  by the central limit theorem, as discussed in Sec. III-A. Meanwhile, different entries of  $\mathbf{x}_{k,b}^{(t)}$  are uncorrelated as  $\mathbf{A}$  is an IID random matrix. Utilizing the modeling of  $\mathbf{x}_{k,b}^{(t)} \sim \mathcal{N}(\mathbf{0}_M, \mathbf{I}_M)$ , we apply the Bussgang theorem to each quantized sub-vector,  $\mathbf{q}_{k,b}^{(t)} = \mathbf{Q}(\mathbf{x}_{k,b}^{(t)})$ , which yields the following proposition:

*Proposition 1:* Suppose that  $\mathbf{Q}(x)$  is a scalar quantizer optimized for the distribution of  $x \sim \mathcal{N}(0, 1)$ . If  $\mathbf{x}_{k,b}^{(t)} \sim \mathcal{N}(\mathbf{0}_M, \mathbf{I}_M)$ , the following decomposition holds:

$$\mathbf{Q}(\mathbf{x}_{k,b}^{(t)}) = \gamma_Q \mathbf{x}_{k,b}^{(t)} + \mathbf{d}_{k,b}^{(t)}, \quad (20)$$



where  $\mathbf{d}_{k,b}^{(t)}$  is a quantization distortion uncorrelated with  $\mathbf{x}_{k,b}^{(t)}$ , and  $\gamma_Q$  and  $\psi_Q$  are quantizer-dependent constants defined as

$$\gamma_Q = \sum_{i=1}^{2^Q} \frac{q_i}{\sqrt{2\pi}} \left\{ \exp\left(-\frac{\tau_{i-1}^2}{2}\right) - \exp\left(-\frac{\tau_i^2}{2}\right) \right\}, \quad (21)$$

and

$$\psi_Q = \sum_{i=1}^{2^Q} q_i^2 \int_{\tau_{i-1}}^{\tau_i} \frac{1}{\sqrt{2\pi}} e^{-\frac{u^2}{2}} du, \quad (22)$$

respectively. The distortion  $\mathbf{d}_{k,b}^{(t)}$  has zero mean and the covariance of  $\mathbf{R}_{\mathbf{d}_{k,b}^{(t)}} = (\psi_Q - \gamma_Q^2)\mathbf{I}_M$ .

*Proof:* Let  $\mathbf{q}_{k,b}^{(t)} = \mathbf{Q}(\mathbf{x}_{k,b}^{(t)})$ . The Bussgang theorem in [28] shows that if  $\mathbf{x}_{k,b}^{(t)} \sim \mathcal{N}(\mathbf{0}_M, \mathbf{I}_M)$ , we have  $\mathbf{q}_{k,b}^{(t)} = \gamma_Q \mathbf{x}_{k,b}^{(t)} + \mathbf{d}_{k,b}^{(t)}$ , where  $\mathbf{d}_{k,b}^{(t)}$  is a quantization distortion uncorrelated with  $\mathbf{x}_{k,b}^{(t)}$  and  $\gamma_Q$  is a quantizer-dependent constant defined in (21) as derived in [35]. If the scalar quantizer  $\mathbf{Q}(\cdot)$  is optimized for  $\mathcal{N}(0, 1)$ , the distortion  $\mathbf{d}_{k,b}^{(t)}$  has zero mean because both  $\mathbf{q}_{k,b}^{(t)}$  and  $\mathbf{x}_{k,b}^{(t)}$  have zero mean. In addition, since  $\mathbf{x}_{k,b}^{(t)}$  and  $\mathbf{d}_{k,b}^{(t)}$  are uncorrelated, the covariance of  $\mathbf{q}_{k,b}^{(t)}$  is obtained as  $\mathbf{R}_{\mathbf{q}_{k,b}^{(t)}} = \gamma_Q^2 \mathbf{I}_M + \mathbf{R}_{\mathbf{d}_{k,b}^{(t)}}$ , where  $\mathbf{R}_{\mathbf{d}_{k,b}^{(t)}}$  is the covariance of  $\mathbf{d}_{k,b}^{(t)}$ . It is also easy to show that  $\mathbf{R}_{\mathbf{q}_{k,b}^{(t)}} = \psi_Q \mathbf{I}_M$  when  $\mathbf{x}_{k,b}^{(t)} \sim \mathcal{N}(\mathbf{0}_M, \mathbf{I}_M)$ , where  $\psi_Q$  is a quantizer-dependent constant defined in (22). Combining these results yields  $\mathbf{R}_{\mathbf{d}_{k,b}^{(t)}} = (\psi_Q - \gamma_Q^2)\mathbf{I}_M$ . ■

Utilizing the result in Proposition 1, we aggregate the quantized sub-vectors by assigning a special weight  $\frac{\rho_k^{(t)}}{\gamma_Q \alpha_{k,b}^{(t)}}$  to  $\mathbf{q}_{k,b}^{(t)}$  as follows:

$$\tilde{\mathbf{q}}_{\mathcal{K}_g,b}^{(t)} = \sum_{k \in \mathcal{K}_g} \frac{\rho_k^{(t)}}{\gamma_Q \alpha_{k,b}^{(t)}} \mathbf{q}_{k,b}^{(t)} = \sum_{k \in \mathcal{K}_g} \frac{\rho_k^{(t)}}{\gamma_Q \alpha_{k,b}^{(t)}} (\gamma_Q \alpha_{k,b}^{(t)} \mathbf{A} \mathbf{g}_{k,b}^{(t)} + \mathbf{d}_{k,b}^{(t)}) = \mathbf{A} \mathbf{g}_{\mathcal{K}_g,b}^{(t)} + \tilde{\mathbf{d}}_{\mathcal{K}_g,b}^{(t)}, \quad (23)$$

where  $\tilde{\mathbf{d}}_{\mathcal{K}_g,b}^{(t)} = \sum_{k \in \mathcal{K}_g} \frac{\rho_k^{(t)}}{\gamma_Q \alpha_{k,b}^{(t)}} \mathbf{d}_{k,b}^{(t)}$  is an effective distortion uncorrelated with  $\mathbf{g}_{\mathcal{K}_g,b}^{(t)}$ . As can be seen in (23), estimating the aggregated sub-vector,  $\mathbf{g}_{\mathcal{K}_g,b}^{(t)}$ , from the observation of  $\tilde{\mathbf{q}}_{\mathcal{K}_g,b}^{(t)}$  is formulated a standard CS recovery problem with noise. Nevertheless, it is still difficult to find the exact MMSE solution of this problem as the distribution of  $\tilde{\mathbf{d}}_{\mathcal{K}_g,b}^{(t)}$  is unknown in general. To circumvent this difficulty, we assume that the correlation among distortions from different gradient sub-vectors is negligible which can be justified when local gradient sub-vectors from different devices are computed from different training samples. We then model the effective distortion as a Gaussian random vector with consistent mean and covariance. Under this strategy, the effective distortion  $\tilde{\mathbf{d}}_{\mathcal{K}_g,b}^{(t)}$  becomes an additive white Gaussian noise (AWGN) with the variance of

$$\nu_{g,b}^{(t)} = \frac{\psi_Q - \gamma_Q^2}{\gamma_Q^2} \sum_{k \in \mathcal{K}_g} \left( \frac{\rho_k^{(t)}}{\alpha_{k,b}^{(t)}} \right)^2. \quad (24)$$

Based on the AWGN modeling of the effective distortion, we solve each CS recovery problem of (23) by employing the original EM-GAMP algorithm in [26]. Unlike the Q-EM-GAMP algorithm in the estimate-and-aggregate strategy, the original EM-GAMP algorithm is directly applied to an *unquantized* linear observation of  $\tilde{\mathbf{q}}_{\mathcal{K}_g,b}^{(t)}$  while assuming IID Bernoulli Gaussian-mixture prior for the aggregated sub-vector,  $\mathbf{g}_{\mathcal{K}_g,b}^{(t)}$ . Another key difference is that in the problem of (23), we have a *noisy* observation due to the presence of the effective distortion  $\tilde{\mathbf{d}}_{\mathcal{K}_g,b}^{(t)}$ ; thereby, the effect of the noise is taken into account when employing the EM-GAMP algorithm to solve (23). We denote the EM-GAMP algorithm utilized in the aggregate-and-estimate strategy by  $\text{EMGAMP}(\tilde{\mathbf{q}}_{\mathcal{K}_g,b}^{(t)}, \nu_{g,b}^{(t)}, \mathbf{A})$ , where  $\tilde{\mathbf{q}}_{\mathcal{K}_g,b}^{(t)}$  is a linear observation,  $\nu_{g,b}^{(t)}$  is a AWGN variance, and  $\mathbf{A}$  is a sensing matrix. This EM-GAMP algorithm is also obtained by replacing Step 7 and Step 8 in **Procedure 2** with  $\hat{x}_m^{\text{post}} = (\hat{p}_m \nu_d + q_m \nu_{p_m}) / (\nu_{p_m} + \nu_d)$  and  $\nu_{x_m}^{\text{post}} = (1/\nu_{p_m} + 1/\nu_d)^{-1}$ , respectively, where  $\nu_d$  is an input noise variance. Finally, we reconstruct the global gradient vector by aggregating the estimates of the aggregated sub-vectors. Let  $\hat{\mathbf{g}}_{\mathcal{K}_g,b}^{(t)}$  be the estimate of  $\mathbf{g}_{\mathcal{K}_g,b}^{(t)}$  computed by applying the EM-GAMP algorithm to  $\tilde{\mathbf{q}}_{\mathcal{K}_g,b}^{(t)}$ . Then the global gradient vector in (5) is reconstructed as  $\hat{\mathbf{g}}_{\mathcal{K}}^{(t)} = \sum_{g=1}^G \hat{\mathbf{g}}_{\mathcal{K}_g}^{(t)}$ , where  $\hat{\mathbf{g}}_{\mathcal{K}_g}^{(t)} = \text{Concatenate}(\{\hat{\mathbf{g}}_{\mathcal{K}_g,b}^{(t)}\}_{b=1}^B)$ . The overall gradient reconstruction process of the aggregate-and-estimate strategy is summarized in Steps 16–20 of **Procedure 1**.

A key benefit of the aggregate-and-estimate strategy is that it requires a lower complexity than the estimate-and-aggregate strategy when  $G < K$  because the aggregate-and-estimate strategy solves only  $GB$  CS recovery problems to reconstruct the global gradient vector. Another key benefit is that the aggregate-and-estimate strategy allows the PS to control the complexity of the gradient reconstruction process by adjusting the number of sub-vectors per group. It is worth mentioning that the complexity reduction achieved by this strategy comes at the cost of reconstruction accuracy because the number of non-zero values in  $\mathbf{g}_{\mathcal{K}_g,b}^{(t)}$  is higher than that in  $\mathbf{g}_{k,b}^{(t)}$ , which degrades the accuracy of the CS recovery process. In particular, the degradation in the reconstruction accuracy becomes severe as the number of sub-vectors per group increases because the larger the number of the sub-vectors per group, the larger the number of non-zero values in  $\mathbf{g}_{\mathcal{K}_g,b}^{(t)}$ . Therefore, when employing the aggregate-and-estimate strategy, there is a trade-off between the accuracy and the complexity of the gradient reconstruction.

## V. PERFORMANCE ANALYSIS

In this section, we analyze the gradient reconstruction error as well as the convergence rate of FedQCS. We first characterize an upper bound for the reconstruction error achieved by FedQCS with the aggregate-and-estimate strategy in Sec. IV-B. We then characterize the convergence rate of FedQCS under the consideration of the reconstruction error bound.

### A. Reconstruction Error Analysis

In this analysis, we characterize an upper bound of the gradient reconstruction error in FedQCS. We particularly aim at analyzing the performance of the aggregate-and-estimate strategy with  $G = 1$  which provides the worst-case performance as discussed in Sec. IV-B. We also make some useful assumptions for mathematical tractability of the reconstruction error analysis, even if these assumptions are not necessary for employing the proposed gradient reconstruction strategies. The assumptions made in our analysis are described below.

*Assumption 1:* Every local gradient sub-vector,  $\mathbf{g}_{k,b}^{(t)}$ , follows a Bernoulli Gaussian-mixture distribution in (11) which is already known at the PS.

*Assumption 2:* Every quantization distortion,  $\mathbf{d}_{k,b}^{(t)}$ , follows a Gaussian distribution.

Under Assumptions 1 and 2, we characterize an upper bound of the MSE of the global gradient vector as given in the following theorem:

*Theorem 1:* Suppose that Assumptions 1 and 2 hold. In the asymptotic regime of  $N \rightarrow \infty$  and  $N/M \rightarrow R$  for a fixed ratio  $R \geq 1$ , the global gradient vector reconstructed by the aggregate-and-estimate strategy with  $G = 1$  satisfies the following MSE bound:

$$\mathbb{E}[\|\mathbf{g}_{\mathcal{K}}^{(t)} - \hat{\mathbf{g}}_{\mathcal{K}}^{(t)}\|^2] \leq N \sum_{b=1}^B \tilde{\nu}_{\mathcal{K},b}^{(t)} \left( 1 - \frac{\tilde{\nu}_{\mathcal{K},b}^{(t)}}{R\tilde{\nu}_{\mathcal{K},b}^{(t)} + \kappa_Q(\tilde{\nu}_{\mathcal{K},b}^{(t)} + \tilde{\mu}_{\text{sq},\mathcal{K},b}^{(t)})} \right), \quad (25)$$

where  $\tilde{\mu}_{\text{sq},\mathcal{K},b}^{(t)} = \sum_{k=1}^K (\rho_k^{(t)} \mu_{\mathbf{g}_{k,b}}^{(t)})^2$  and  $\tilde{\nu}_{\mathcal{K},b}^{(t)} = \sum_{k=1}^K (\rho_k^{(t)})^2 \nu_{\mathbf{g}_{k,b}}^{(t)}$ , provided that  $\mathbf{g}_{k,b}^{(t)}$  is an IID random vector with mean  $\mu_{\mathbf{g}_{k,b}}^{(t)}$  and variance  $\nu_{\mathbf{g}_{k,b}}^{(t)}$ .

*Proof:* See Appendix A. ■

Theorem 1 shows how the reconstruction error in FedQCS depends on the dimension reduction ratio  $R$ , the quantization function (captured by  $\kappa_Q$ ), and the distribution of the gradient vector (captured by  $\tilde{\mu}_{\text{sq},\mathcal{K},b}^{(t)}$  and  $\tilde{\nu}_{\mathcal{K},b}^{(t)}$ ). Since  $\kappa_Q \rightarrow 0$  as  $Q \rightarrow \infty$ , Theorem 1 also demonstrates that the reconstruction error in FedQCS vanishes as  $Q \rightarrow \infty$  and  $R \rightarrow 1$ . This result implies that perfect

reconstruction of the global gradient vector is feasible at the PS when employing FedQCS with  $Q = \infty$  and  $R = 1$ , which also coincides with our intuition.

### B. Convergence Rate Analysis

In this analysis, we characterize the convergence rate of FedQCS operating with the SGD algorithm. We particularly make the following assumptions not only to provide mathematical tractability for the convergence rate analysis, but also to connect this analysis with the reconstruction error analysis in Sec. V-A.

*Assumption 3:* The loss function  $F(\mathbf{w})$  is  $\beta$ -smooth and is lower bounded by some constant  $F(\mathbf{w}^*)$ , i.e.,  $F(\mathbf{w}) \geq F(\mathbf{w}^*)$ ,  $\forall \mathbf{w} \in \mathbb{R}^N$ .

*Assumption 4:* For a given parameter vector  $\mathbf{w}_t$ , the global gradient vector in (5) is unbiased and has bounded variance, i.e.,  $\mathbb{E}[\mathbf{g}_{\mathcal{K}}^{(t)} | \mathbf{w}_t] = \nabla F(\mathbf{w}_t)$  and  $\mathbb{E}[\|\mathbf{g}_{\mathcal{K}}^{(t)} - \nabla F(\mathbf{w}_t)\|^2 | \mathbf{w}_t] \leq \sigma^2$ , for all  $t \in \{1, \dots, T\}$ .

*Assumption 5:* The squared reconstruction error is upper bounded by the squared norm of the true gradient vector with some scaling factor  $\epsilon < 1$ , i.e.,  $\|\hat{\mathbf{g}}_{\mathcal{K}}^{(t)} - \mathbf{g}_{\mathcal{K}}^{(t)}\|^2 \leq \epsilon \|\nabla F(\mathbf{w}_t)\|^2$ , for all  $t \in \{1, \dots, T\}$ .

We would like to make some important comments on the above assumptions. Assumption 3 is standard for analyzing the convergence properties of a family of gradient descent algorithms (e.g., [12], [13]). Assumption 4 is useful to capture the impact of the mini-batch size as well as the block sparsification level  $S$ . A similar assumption is also considered in the literature (e.g., [12]). More precisely, the variance bound  $\sigma^2$  can be made smaller by increasing both the mini-batch size and the sparsification level. Assumption 5 is particularly relevant to FedQCS because the recovery strategies in FedQCS aim at reducing the squared estimation error of the global gradient vector. From Theorem 1, we have already shown that the expectation of the squared reconstruction error vanishes as  $Q \rightarrow \infty$  and  $R \rightarrow 1$ , implying that  $\epsilon \rightarrow 0$  as  $Q \rightarrow \infty$  and  $R \rightarrow 1$ . In Sec. VI, we will also demonstrate that the scaling factor  $\epsilon$  is extremely small under practical scenarios (i.e.,  $\epsilon \ll 1$ ).

Under Assumptions 3  $\sim$  5, we characterize the convergence rate of FedQCS with a fixed learning rate  $\eta_t = \frac{(1-\sqrt{\epsilon})}{2\beta(1+\epsilon)\sqrt{T}}$ , as given in the following theorem:

*Theorem 2:* Under Assumptions 3 ~ 5, FedQCS with a fixed learning rate  $\eta_t = \frac{(1-\sqrt{\epsilon})}{2\beta(1+\epsilon)\sqrt{T}}$  satisfies the following bound:

$$\mathbb{E} \left[ \frac{1}{T} \sum_{t=1}^T \|\nabla F(\mathbf{w}_t)\|^2 \right] \leq \frac{1}{\sqrt{T}} \left[ \frac{4\beta(1+\epsilon)}{(1-\sqrt{\epsilon})^2} \{F(\mathbf{w}_1) - F(\mathbf{w}^*)\} + \frac{\sigma^2}{1+\epsilon} \right]. \quad (26)$$

*Proof:* See Appendix B. ■

Theorem 2 demonstrates that FedQCS converges to a stationary point of the loss function if the initial loss,  $F(\mathbf{w}_1) - F(\mathbf{w}^*)$ , the variance of the global gradient vector (captured by  $\sigma^2$ ), and the reconstruction error (captured by  $\epsilon$ ) are finite. It is also shown that the convergence rate of FedQCS has the order of  $\mathcal{O}(\frac{1}{\sqrt{T}})$  which is the same as that of the original SGD algorithm. The scaling factor of the convergence rate decreases as both  $\epsilon$  and  $\sigma^2$  reduces; thereby, the convergence rate of FedQCS improves as  $Q \rightarrow \infty$  and  $R \rightarrow 1$  provided that both the mini-batch size and the sparsification level are sufficiently large.

## VI. SIMULATION RESULTS

In this section, we demonstrate the superiority of FedQCS over the existing federated learning frameworks, using simulations. In these simulations, we consider an image classification task using the publicly accessible MNIST dataset, where each data sample is a  $28 \times 28$  grayscale image representing a handwritten digit from 0 to 9 [29]. The MNIST dataset consists of the 60,000 training data samples and the 10,000 test data samples. We set the number of wireless devices as  $K = 30$  and consider *non-IID* distribution of the training data samples over the devices. In particular, we construct the local training data set of device  $k$ ,  $\mathcal{D}_k$ , by randomly selecting 1,000 training data samples labeled with  $d_k = \lfloor \frac{k-1}{K/10} \rfloor$  in the MNIST dataset. A global model on the PS is assumed to be a neural network that consists of 784 input nodes, a single hidden layer with 20 hidden nodes, and 10 output nodes. The activation functions of the hidden layer and the output layer are set as the rectified linear unit and the softmax function, respectively. The total number of the weights in the global model is  $\bar{N} = 15,910$ . To train the global model, we adopt the Adam optimizer in [30] with a learning rate 0.003 and cross-entropy loss function. We also consider *stochastic* gradient descent setting by assuming that  $|\mathcal{D}_k^{(t)}| = 1$ , for all  $k \in \mathcal{K}$  and  $t \in \{1, \dots, T\}$ .

For performance evaluation, we mainly consider two performance metrics: (i) classification accuracy and (ii) normalized MSE (NMSE), defined as  $\|\mathbf{g}_{\mathcal{K}}^{(t)} - \hat{\mathbf{g}}_{\mathcal{K}}^{(t)}\|^2 / \|\mathbf{g}_{\mathcal{K}}^{(t)}\|^2$ . Federated learning frameworks considered for performance comparison are described below.

- *FedQCS-EA and FedQCS-AE*: FedQCS-EA and FedQCS-AE are the proposed FedQCS using the estimate-and-aggregate strategy in Sec. IV-A and the aggregate-and-estimate strategy in Sec. IV-B, respectively. The Q-EM-GAMP algorithm and the EM-GAMP algorithm adopted in these strategies are initialized as follows: We randomly set an initial estimate as  $\hat{g}_n \sim \mathcal{N}(0, \frac{M}{N\alpha^2})$ ,  $\forall n \in \{1, \dots, N\}$ , considering the fact that  $\alpha^2 = M/\|\mathbf{g}\|^2$ . We then initialize the parameters  $\boldsymbol{\theta}$  of the Bernoulli Gaussian-mixture model as  $L = 3$ ,  $\lambda_0 = 0.9$ ,  $\lambda_l = \frac{1-\lambda_0}{L}$ ,  $\mu_l = \hat{g}_{\min} + \frac{2l-1}{2L}(\hat{g}_{\max} - \hat{g}_{\min})$ ,  $\phi_l = \frac{1}{12}(\frac{\hat{g}_{\max}-\hat{g}_{\min}}{L})^2$ ,  $\forall l \in \{1, \dots, L\}$ , where  $\hat{g}_{\max} = \max_n g_n$  and  $\hat{g}_{\min} = \min_n g_n$ . We also set  $\tau_{\text{GAMP}} = 10^{-5}$  and  $I_{\text{GAMP}} = 50$  for the stopping criterion.
- *QCS-QIHT*: QCS-QIHT is a simple modification of the QCS-based federated learning framework introduced in [24], [25]. In this modification, we employ the estimate-and-aggregate strategy based on the quantized iterative hard thresholding (QIHT) algorithm in [36], instead of the Q-EM-GAMP algorithm, while utilizing the proposed BQCS compression in Sec. III-A. It is worth mentioning that unlike the Q-EM-GAMP algorithm, the QIHT algorithm requires the knowledge of the sparsity level  $S$ . In this algorithm, we scale the reconstructed gradient vector,  $\hat{\mathbf{g}}_{k,b}^{(t)}$ , using the scaling factor  $\alpha_{k,b}^{(t)}$  in order to make the norm of  $\hat{\mathbf{g}}_{k,b}^{(t)}$  consistent with that of the true gradient vector  $\mathbf{g}_{k,b}^{(t)}$ .
- *QCS-Dither*: QCS-Dither is the existing QCS-based federated learning framework introduced in [23]. This framework employs the gradient compression based on dithered uniform quantization with dimension reduction, while utilizing a simple linear estimator to reconstruct the global gradient vector. Unlike FedQCS and QCS-QIHT, the sensing matrix  $\mathbf{A}$  is determined as the product of the Hadamard and random Rademacher diagonal matrix, as proposed in [23].
- *SignSGD*: SignSGD is the existing federated learning framework introduced in [12]. In SignSGD, each device transmits the sign of each entry of the local gradient vector, then the PS aggregates the received signs of the local gradient entries by a majority vote. For this reason, the communication overhead of SignSGD is  $\bar{N}$  bits per device.

Except for SignSGD, we adopt the block sparsification process with  $B = 10$  and  $S = \lfloor S_{\text{ratio}}N \rfloor$ , where  $S_{\text{ratio}}$  is the ratio of the number of non-zero gradient entries. For FedQCS and QCS-QIHT, we adopt the Lloyd-Max scalar quantizer optimized for  $\mathcal{N}(0, 1)$ .

In Fig. 3, we compare the classification accuracy and the NMSE of different federated learning frameworks with one bit overhead per gradient entry (i.e.,  $\bar{N}$  bits per device). In this simulation,

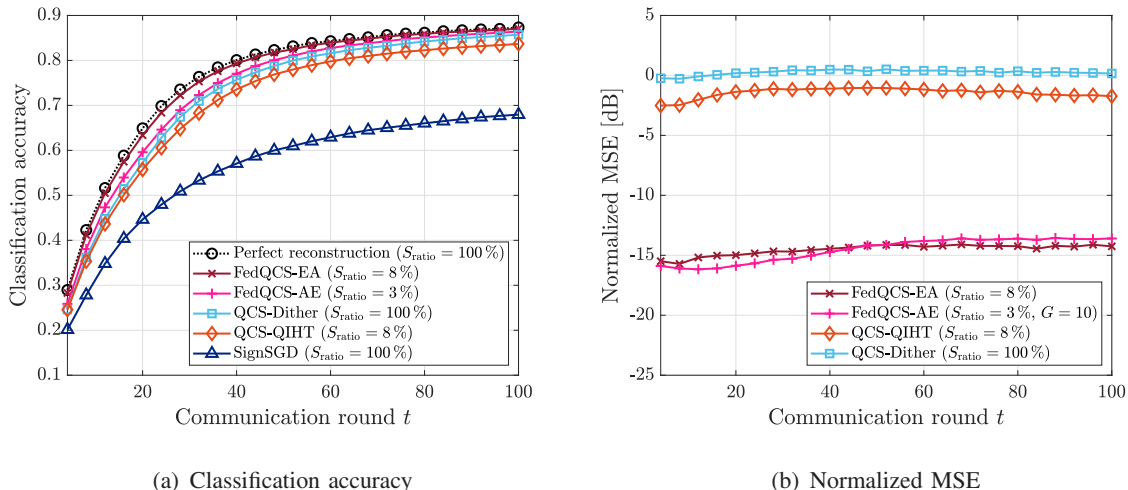


Fig. 3. Performance comparison of different federated learning frameworks with one bit overhead per gradient entry.

we set  $(R, Q) = (3, 3)$  for all the QCS-based frameworks. As a performance benchmark, we also plot the optimal performance achieved when the global gradient vector is perfectly reconstructed at the PS, requiring the communication overhead of 32 bits per gradient entry when employing floating-point representation. Fig. 3(a) shows that FedQCS-EA achieves the almost same accuracy as perfect reconstruction while requiring 32 times less communication overhead. This result implies that the proposed federated learning framework enables not only significant reduction in the communication overhead, but also *almost lossless* reconstruction of the global gradient vector at the PS. It is also shown that both FedQCS-EA and FedQCS-AE achieve a higher classification accuracy (see Fig. 3(a)) as well as a lower NMSE (see Fig. 3(b)) compared to the existing frameworks requiring the same overhead. The performance gain of FedQCS over both QCS-QIHT and QCS-Dither demonstrates the superiority of the proposed recovery strategies over the QIHT algorithm in [24], [25] or a simple linear estimator in [23]. Meanwhile, the performance gain of FedQCS over SignSGD demonstrates that the proposed BQCS compression is more effective than one-bit gradient compression by exploiting the sparse property of the local gradients.

In Fig. 4, we compare the classification accuracy of different QCS-based federated learning frameworks with various communication overheads. In this simulation, we set  $R = 3$  and increase the value of  $Q$  from 1 to 6, which corresponds to 1/3-bit overhead to 2-bit overhead per gradient entry. Fig. 4 shows that FedQCS achieves the highest classification accuracy regardless of the communication overhead. Meanwhile, the performance gain of FedQCS over the existing frame-

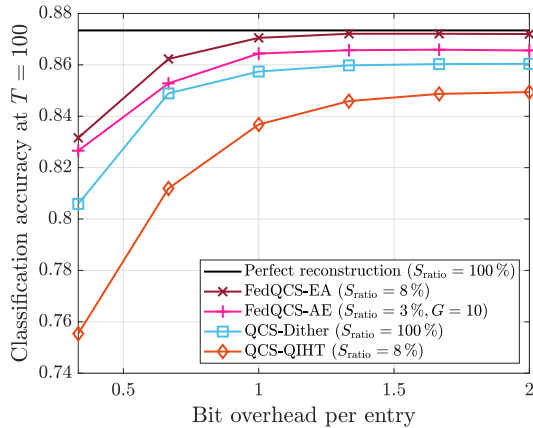


Fig. 4. The classification accuracy vs. communication overhead for different federated learning frameworks.

works increases as the communication overhead reduces. This result demonstrates the robustness of FedQCS against the increase in the compression ratio. Another interesting observation is that the classification accuracy of all the frameworks saturates as the communication overhead increases. This phenomenon implies that if the number of quantization bits becomes sufficiently large (e.g.,  $Q = 4$ ), there is no significant reduction in the quantization error.

In Table I, we compare the computational complexity of different QCS-based federated learning frameworks. Table I shows that FedQCS-EA has a similar complexity order with QCS-QIHT, while providing additional performance gain as can be seen in Fig. 3. It is also shown that FedQCS-AE requires a less complexity than FedQCS-EA; this complexity reduction increases with the number of aggregation groups,  $G$ . In particular, when  $G = 1$ , the complexity of FedQCS-EA is  $K$  times lower than that of FedQCS-AE. This complexity reduction, however, is attained at the cost of the classification accuracy (see Fig. 3), as also discussed in Sec. IV-B. Although QCS-Dither has the lowest complexity order, it suffers from performance degradation in terms of both classification accuracy and NMSE (see Fig. 3), while requiring additional signaling overhead as discussed in **Remark 1**.

In Fig. 5, we evaluate the classification accuracy of different QCS-based federated learning frameworks with various choices of  $(R, Q)$ . Fig. 5 shows that FedQCS-EA achieves the highest classification accuracy regardless of the choice of  $(R, Q)$ . Unlike FedQCS-EA, the performance of the existing QCS-based frameworks changes significantly depending on the choice of  $(R, Q)$ . This result demonstrates the robustness of FedQCS-EA against the changes in  $(R, Q)$  compared to the existing QCS-based frameworks. Another interesting observation is that there is the

TABLE I  
COMPLEXITY ORDER REQUIRED BY DIFFERENT  
QCS-BASED FEDERATED LEARNING FRAMEWORKS

Algorithm	Complexity Order
QCS-Dither	$\mathcal{O}(BMN)$
QCS-QIHT	$\mathcal{O}(KBMNI_{\text{QIHT}})$
FedQCS-EA	$\mathcal{O}(KBMNI_{\text{GAMP}})$
FedQCS-AE	$\mathcal{O}(GBMNI_{\text{GAMP}})$



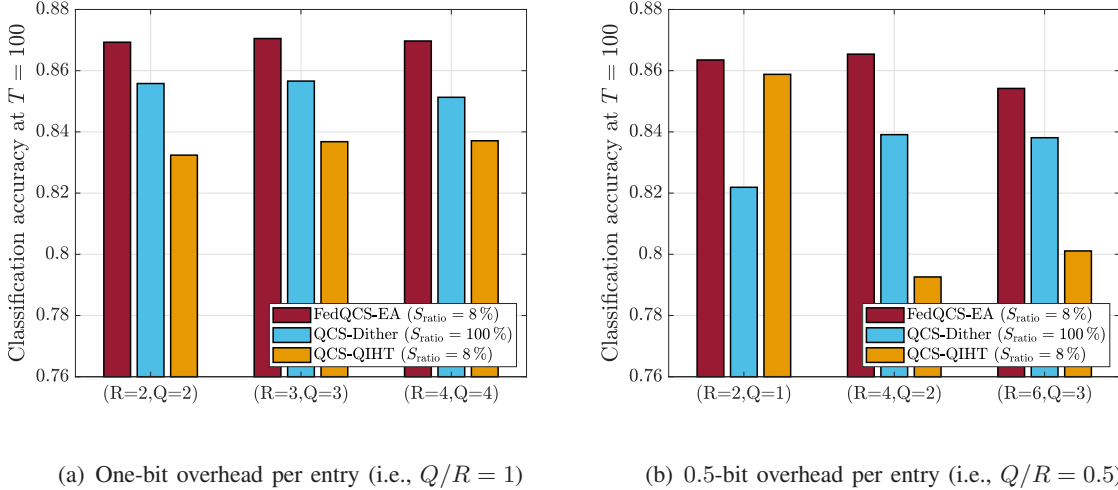


Fig. 5. The classification accuracy of different federated learning frameworks with various choices of  $(R, Q)$ .

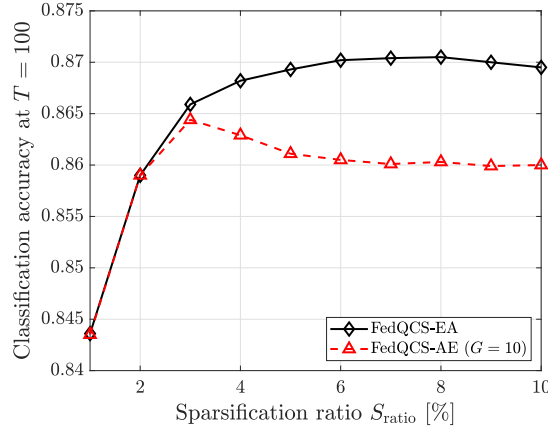


Fig. 6. The classification accuracy of FedQCS with different values of  $S_{\text{ratio}}$  when  $(R, Q) = (3, 3)$ .

optimal choice of  $(R, Q)$  that provides the highest classification accuracy even for the same communication overhead (i.e., even for a fixed ratio  $Q/R$ ). The reason behind this phenomenon is that the performance of the QCS-based compression depends on two types of errors: *compression error* and *quantization error*, determined by  $R$  and  $Q$ , respectively. For example, for FedQCS-EA with  $Q/R = 1$ , the performance with  $(R, Q) = (2, 2)$  is shown to be worse than that with  $(R, Q) = (3, 3)$  because the effect of the quantization error becomes dominant when  $Q = 2$ . Similarly, the performance with  $(R, Q) = (4, 4)$  is shown to be worse than that with  $(R, Q) = (3, 3)$  because the effect of the compression error becomes dominant when  $R = 4$ . Therefore, for a fixed communication overhead, a judicious optimization of  $R$  and  $Q$  is still necessary to maximize the performance of the QCS-based gradient compression.

In Fig. 6, we evaluate the classification accuracy of FedQCS with different values of  $S_{\text{ratio}}$

when  $(R, Q) = (3, 3)$ . Fig. 6 shows that both FedQCS-EA and FedQCS-AE provide the highest classification accuracy at a certain sparsification ratio. The reason behind this phenomenon is that increasing  $S_{\text{ratio}}$  allows the wireless devices to convey a larger number of gradient entries to the PS, while increasing the number of non-zero entries which leads to degradation in the reconstruction performance at the PS. Therefore, there is the trade-off between the amount of the information sent by the devices and the accuracy of the reconstruction at the PS. It is also shown that as  $S_{\text{ratio}}$  increases, the accuracy of FedQCS-AE degrades earlier than that of the parallel recovery and therefore has a lower value of the optimal sparsification ratio. This coincides with our intuition because the aggregate-and-estimate strategy has a large number of non-zero gradient entries due to the aggregation of the gradient sub-vectors before the estimation, as discussed in Sec. IV-B.

## VII. CONCLUSION

In this paper, we have presented FedQCS, a communication-efficient federated learning framework based on QCS. One prominent feature of FedQCS is that it provides flexible communication overhead that can be made even less than one bit per gradient entry. Another key feature is that gradient reconstruction strategies of FedQCS enable accurate gradient reconstruction at the PS by computing an approximate MMSE estimate of local gradients. By analyzing the reconstruction error as well as the convergence rate of FedQCS, we have demonstrated that the convergence of FedQCS is guaranteed with the rate of  $\mathcal{O}(\frac{1}{\sqrt{T}})$ . Using the MNIST dataset, we have demonstrated that FedQCS with one bit overhead per gradient entry suffices to attain almost identical performance as perfect reconstruction with no compression. An important direction of future research is to extend the presented framework for the use in wireless multiple access channels which enable further reduction in the communication overhead by allowing the simultaneous transmission of the quantized gradient vectors. In this direction, it would also be important to optimize device scheduling and power control by taking into account different locations and channel conditions of the devices in wireless networks.

## APPENDIX A

### PROOF OF THEOREM 1

In this analysis, we omit the index  $t$  for the sake of brevity. Consider the asymptotic regime of  $N \rightarrow \infty$  and  $N/M \rightarrow R$  for a fixed ratio  $R \geq 1$ . When employing the joint recovery

strategy with  $G = 1$  and large  $N$ , a gradient reconstruction problem in (23) is formulated as  $\tilde{\mathbf{q}}_{\mathcal{K},b} = \mathbf{A}\mathbf{g}_{\mathcal{K},b} + \tilde{\mathbf{d}}_{\mathcal{K},b}$ . As discussed in Sec. IV-B, we have  $\tilde{\mathbf{d}}_{\mathcal{K},b} \sim \mathcal{N}(\mathbf{0}_M, \xi_{\mathcal{K},b}\mathbf{I}_M)$  with  $\xi_{\mathcal{K},b} = \kappa_Q \sum_{k=1}^K \rho_k^2 / \alpha_{k,b}^2$  under Assumptions 1 and 2 with large  $N$ . Let  $\mu_{\mathbf{g}_{k,b}}$  and  $\nu_{\mathbf{g}_{k,b}}$  be the mean and the variance of the entry of  $\mathbf{g}_{k,b}$ , respectively. Then in the asymptotic regime, we have  $1/\alpha_{k,b}^2 = \|\mathbf{g}_{k,b}\|^2/M = \nu_{\mathbf{g}_{k,b}} + \mu_{\mathbf{g}_{k,b}}^2$  under Assumption 1. Utilizing the above facts, the distortion variance  $\xi_{\mathcal{K},b}$  is asymptotically given by

$$\xi_{\mathcal{K},b} = \kappa_Q \sum_{k=1}^K \rho_k^2 (\nu_{\mathbf{g}_{k,b}} + \mu_{\mathbf{g}_{k,b}}^2) = \kappa_Q (\tilde{\nu}_{\mathcal{K},b} + \tilde{\mu}_{\text{sq},\mathcal{K},b}), \quad (27)$$

where  $\tilde{\nu}_{\mathcal{K},b} = \sum_{k=1}^K \rho_k^2 \nu_{\mathbf{g}_{k,b}}$  and  $\tilde{\mu}_{\text{sq},\mathcal{K},b} = \sum_{k=1}^K \rho_k^2 \mu_{\mathbf{g}_{k,b}}^2$ . Under Assumption 1, the EM-GAMP algorithm applied to estimate the  $\mathbf{g}_{\mathcal{K},b}$  from  $\tilde{\mathbf{q}}_{\mathcal{K},b}$  exactly behaves like the GAMP algorithm in [37]–[39]. Let  $\hat{\mathbf{g}}_{\mathcal{K},b}$  be the estimate of  $\mathbf{g}_{\mathcal{K},b}$  obtained by the EM-GAMP algorithm, and  $\hat{\mathbf{g}}_{\mathcal{K},b}^{\text{LMMSE}}$  be the *linear* MMSE (LMMSE) estimate of  $\mathbf{g}_{\mathcal{K},b}$  for a given observation  $\tilde{\mathbf{q}}_{\mathcal{K},b}$ . The analysis in [37]–[39] shows that in the asymptotic regime, the GAMP algorithm applied to estimate  $\mathbf{g}_{\mathcal{K},b}$  from an AWGN observation of  $\mathbf{A}\mathbf{g}_{\mathcal{K},b}$  is characterized by a scalar state evolution; if this state evolution has a unique fixed point, the solution of the GAMP algorithm converges to the MMSE estimate of  $\mathbf{g}_{\mathcal{K},b}$  for the given observation. The above discussions imply that in the asymptotic regime, the MSE of  $\hat{\mathbf{g}}_{\mathcal{K},b}$  is lower than the MSE of  $\hat{\mathbf{g}}_{\mathcal{K},b}^{\text{LMMSE}}$ , i.e.,

$$\mathbb{E}[\|\mathbf{g}_{\mathcal{K},b} - \hat{\mathbf{g}}_{\mathcal{K},b}\|^2] \leq \mathbb{E}[\|\mathbf{g}_{\mathcal{K},b} - \hat{\mathbf{g}}_{\mathcal{K},b}^{\text{LMMSE}}\|^2]. \quad (28)$$

Under Assumption 1 with large  $N$ ,  $\tilde{\mathbf{d}}_{\mathcal{K},b}$  is uncorrelated with  $\mathbf{g}_{\mathcal{K},b}$  by the Bussgang theorem. In addition, the variance of  $\mathbf{g}_{\mathcal{K},b}$  is computed as  $\tilde{\nu}_{\mathcal{K},b}$  under Assumption 1. Utilizing these facts, the MSE of  $\hat{\mathbf{g}}_{\mathcal{K},b}^{\text{LMMSE}}$  can be readily computed as [40]

$$\begin{aligned} \mathbb{E}[\|\mathbf{g}_{\mathcal{K},b} - \hat{\mathbf{g}}_{\mathcal{K},b}^{\text{LMMSE}}\|^2] &= \tilde{\nu}_{\mathcal{K},b} \text{Tr} \left[ \mathbf{I}_N - \tilde{\nu}_{\mathcal{K},b} \mathbf{A}^\top (\tilde{\nu}_{\mathcal{K},b} \mathbf{A} \mathbf{A}^\top + \xi_{\mathcal{K},b} \mathbf{I}_M)^{-1} \mathbf{A} \right] \\ &\stackrel{(a)}{=} \tilde{\nu}_{\mathcal{K},b} N \left( 1 - \frac{\tilde{\nu}_{\mathcal{K},b}}{R\tilde{\nu}_{\mathcal{K},b} + \xi_{\mathcal{K},b}} \right), \end{aligned} \quad (29)$$

where the equality (a) holds because  $\mathbf{A} \mathbf{A}^\top = R\mathbf{I}_M$  in the asymptotic regime from  $(\mathbf{A})_{m,n} \sim \mathcal{N}(0, 1/M)$ . Since  $\mathbf{g}_{\mathcal{K}}$  is obtained by concatenating the sub-vectors  $\{\mathbf{g}_{\mathcal{K},b}\}_{b=1}^B$ , we have

$$\mathbb{E}[\|\mathbf{g}_{\mathcal{K}} - \hat{\mathbf{g}}_{\mathcal{K}}\|^2] = \sum_{b=1}^B \mathbb{E}[\|\mathbf{g}_{\mathcal{K},b} - \hat{\mathbf{g}}_{\mathcal{K},b}\|^2]. \quad (30)$$

Plugging (27)–(29) into (30) gives the result in (25).

APPENDIX B  
PROOF OF THEOREM 2

Under Assumption 3, the improvement of the loss function at iteration  $t$  satisfies

$$\begin{aligned} F(\mathbf{w}_{t+1}) - F(\mathbf{w}_t) &\leq \nabla F(\mathbf{w}_t)^\top (\mathbf{w}_{t+1} - \mathbf{w}_t) + \frac{\beta}{2} \|\mathbf{w}_{t+1} - \mathbf{w}_t\|^2 \\ &\stackrel{(a)}{=} -\eta_t \nabla F(\mathbf{w}_t)^\top (\mathbf{g}_{\mathcal{K}}^{(t)} + \mathbf{e}_t) + \eta_t^2 \frac{\beta}{2} \|\mathbf{g}_{\mathcal{K}}^{(t)} + \mathbf{e}_t\|^2, \end{aligned} \quad (31)$$

where the equality (a) follows from (6) along with  $\mathbf{e}_t = \hat{\mathbf{g}}_{\mathcal{K}}^{(t)} - \mathbf{g}_{\mathcal{K}}^{(t)}$ . From the Cauchy–Schwarz inequality, we have  $\nabla F(\mathbf{w}_t)^\top \mathbf{e}_t \geq -\|\nabla F(\mathbf{w}_t)\| \cdot \|\mathbf{e}_t\|$  and  $2\mathbf{e}_t^\top \mathbf{g}_{\mathcal{K}}^{(t)} \leq \|\mathbf{g}_{\mathcal{K}}^{(t)}\|^2 + \|\mathbf{e}_t\|^2$ . Applying these inequalities into (31) yields

$$\begin{aligned} F(\mathbf{w}_{t+1}) - F(\mathbf{w}_t) &\leq -\eta_t \nabla F(\mathbf{w}_t)^\top \mathbf{g}_{\mathcal{K}}^{(t)} + \eta_t \|\nabla F(\mathbf{w}_t)\| \cdot \|\mathbf{e}_t\| + \eta_t^2 \beta \{\|\mathbf{g}_{\mathcal{K}}^{(t)}\|^2 + \|\mathbf{e}_t\|^2\} \\ &\stackrel{(b)}{\leq} -\eta_t \nabla F(\mathbf{w}_t)^\top \mathbf{g}_{\mathcal{K}}^{(t)} + \eta_t \sqrt{\epsilon} \|\nabla F(\mathbf{w}_t)\|^2 + \eta_t^2 \beta \{\|\mathbf{g}_{\mathcal{K}}^{(t)}\|^2 + \epsilon \|\nabla F(\mathbf{w}_t)\|^2\}, \end{aligned} \quad (32)$$

where the inequality (b) holds under Assumption 5. Under Assumption 4, we have  $\mathbb{E}[\mathbf{g}_{\mathcal{K}}^{(t)} | \mathbf{w}_t] = \nabla F(\mathbf{w}_t)$  and  $\mathbb{E}[\|\mathbf{g}_{\mathcal{K}}^{(t)}\|^2 | \mathbf{w}_t] \leq \|\nabla F(\mathbf{w}_t)\|^2 + \sigma^2$ . Therefore, taking the expectation of both sides of the inequality in (32) conditioned on  $\mathbf{w}_t$  yields

$$\begin{aligned} \mathbb{E}[F(\mathbf{w}_{t+1}) - F(\mathbf{w}_t) | \mathbf{w}_t] &\leq -\eta_t (1 - \sqrt{\epsilon}) \|\nabla F(\mathbf{w}_t)\|^2 + \eta_t^2 \beta \{(1 + \epsilon) \|\nabla F(\mathbf{w}_t)\|^2 + \sigma^2\} \\ &= -\eta_t \{(1 - \sqrt{\epsilon}) - \eta_t \beta (1 + \epsilon)\} \|\nabla F(\mathbf{w}_t)\|^2 + \eta_t^2 \beta \sigma^2. \end{aligned} \quad (33)$$

Plugging a fixed learning rate  $\eta_t = \frac{(1 - \sqrt{\epsilon})}{2\beta(1 + \epsilon)\sqrt{T}}$  into (33) yields

$$\begin{aligned} \mathbb{E}[F(\mathbf{w}_{t+1}) - F(\mathbf{w}_t) | \mathbf{w}_t] &\leq -\frac{(1 - \sqrt{\epsilon})^2}{2\beta(1 + \epsilon)\sqrt{T}} \left(1 - \frac{1}{2\sqrt{T}}\right) \|\nabla F(\mathbf{w}_t)\|^2 + \frac{(1 - \sqrt{\epsilon})^2}{4\beta(1 + \epsilon)^2 T} \sigma^2 \\ &\stackrel{(c)}{\leq} -\frac{(1 - \sqrt{\epsilon})^2}{4\beta(1 + \epsilon)\sqrt{T}} \|\nabla F(\mathbf{w}_t)\|^2 + \frac{(1 - \sqrt{\epsilon})^2}{4\beta(1 + \epsilon)^2 T} \sigma^2. \end{aligned} \quad (34)$$

where the inequality (c) follows from  $\frac{1}{2\sqrt{T}} \leq \frac{1}{2}$ . By considering a telescoping sum over the iterations, a lower bound of the initial loss with  $\mathbf{w}_1$  is expressed as

$$\begin{aligned} F(\mathbf{w}_1) - F(\mathbf{w}^*) &\geq F(\mathbf{w}_1) - \mathbb{E}[F(\mathbf{w}_{T+1})] = \sum_{t=1}^T \mathbb{E}[F(\mathbf{w}_t) - F(\mathbf{w}_{t+1})] \\ &\stackrel{(d)}{\geq} \frac{(1 - \sqrt{\epsilon})^2}{4\beta(1 + \epsilon)} \mathbb{E} \left[ \frac{1}{\sqrt{T}} \sum_{t=1}^T \|\nabla F(\mathbf{w}_t)\|^2 \right] - \frac{(1 - \sqrt{\epsilon})^2}{4\beta(1 + \epsilon)^2} \frac{1}{T} \sum_{t=1}^T \sigma^2, \end{aligned} \quad (35)$$

where the expectation is taken over randomness in the trajectory, and the inequality (d) follows from (34). The inequality in (35) can be rewritten as in (26), which completes the proof.

## REFERENCES

- [1] Y. Oh, N. Lee, and Y.-S. Jeon, “Quantized compressed sensing for communication-efficient federated learning,” to be appeared in *Proc. IEEE GLOBECOM Workshops*, Dec. 2021, pp. 1–6.
- [2] J. Konečný, B. H. McMahan, and D. Ramage, “Federated optimization: Distributed optimization beyond the datacenter,” arXiv:1511.03575 [cs.LG], Nov. 2015 [Online] Available: <https://arxiv.org/abs/1511.03575>
- [3] H. B. McMahan, E. Moore, D. Ramage, S. Hampson, and B. A. Arcas “Communication-efficient learning of deep networks from decentralized data,” in *Proc. 20th Int. Conf. Artif. Intell. Statist. (AISTATS)*, 2017, pp. 1273–1282.
- [4] S. Niknam, H. S. Dhillon, and J. H. Reed, “Federated learning for wireless communications: Motivation, opportunities and challenges,” *IEEE Commun. Magazine*, vol. 58, no. 1, pp. 19–25, Jan. 2020.
- [5] G. Zhu, D. Liu, Y. Du, C. You, J. Zhang, and K. Huang, “Toward an intelligent edge: Wireless communication meets machine learning,” *IEEE Commun. Magazine*, vol. 58, no. 1, pp. 19–25, Jan. 2020.
- [6] D. Gündüz, D. B. Kurka, M. Jankowski, M. M. Amiri, E. Ozfatura, and S. Sreekumar, “Communicate to learn at the edge,” *IEEE Commun. Magazine*, vol. 58, no. 12, pp. 14–19, Dec. 2020.
- [7] S. Samarakoon, M. Bennis, W. Saad, and M. Debbah, “Distributed federated learning for ultra-reliable low-latency vehicular communications,” *IEEE Trans. Commun.*, vol. 68, no. 2, pp. 1146–1159, Feb. 2020.
- [8] M. Chen, Z. Yang, W. Saad, C. Yin, H. V. Poor, and S. Cui, “A joint learning and communications framework for federated learning over wireless networks,” *IEEE Trans. Wireless Commun.*, vol. 20, no. 1, pp. 269–283, Jan. 2021.
- [9] Y.-S. Jeon, M. M. Amiri, J. Li, and H. V. Poor “A compressive sensing approach for federated learning over massive MIMO communication systems,” *IEEE Trans. Wireless Commun.*, vol. 20, no. 3, pp. 1990–2004, Mar. 2021.
- [10] J. Konečný, H. B. McMahan, F. X. Yu, P. Richtárik, A. T. Suresh, and D. Bacon, “Federated learning: Strategies for improving communication efficiency,” arXiv:1610.05492v2 [cs.LG], Oct. 2016 [Online] Available: <https://arxiv.org/abs/1610.05492>
- [11] D. Alistarh, J. Li, R. Tomioka, and M. Vojnovic, “QSGD: Randomized quantization for communication-optimal stochastic gradient descent,” in *Advances Neural Inf. Process. Syst. (NeurIPS)*, 2017, pp. 1709–1720.
- [12] J. Bernstein, Y.-X. Wang, K. Azizzadenesheli, and A. Anandkumar, “signSGD: Compressed optimisation for non-convex problems,” in *Int. Conf. Mach. Learn. (ICML)*, 2018, pp. 560–569.
- [13] S. Lee, C. Park, S.-N. Hong, Y. C. Eldar, and N. Lee, “Bayesian federated learning over wireless networks,” arXiv:2012.15486 [eess.SP], Dec. 2020 [Online] Available: <https://arxiv.org/abs/2012.15486>
- [14] N. Shlezinger, M. Chen, Y. C. Eldar, H. V. Poor, and S. Cui, “UVEQFed: Universal vector quantization for federated learning,” *IEEE Trans. Signal Process.*, vol. 69, pp. 500–514, 2021.
- [15] Y. Du, S. Yang, and K. Huang, “High-dimensional stochastic gradient quantization for communication-efficient edge learning,” *IEEE Trans. Signal Process.*, vol. 68, pp. 2128–2142, 2020.
- [16] M. Chen, N. Shlezinger, H. V. Poor, Y. C. Eldar, and S. Cui, “Communication efficient federated learning,” in *Proc. National Academy of Sciences (PNAS)*, vol. 118, no. 17, Apr. 2021.
- [17] W. Huang, Y. Yang, M. Chen, C. Feng, and H. V. Poor, “Wireless network optimization for federated learning with model compression in hybrid VLC/RF systems,” *Entropy*, vol. 23, no. 11, Nov. 2021.
- [18] A. F. Aji and K. Heafield, “Sparse communication for distributed gradient descent,” in *Empirical Methods in Natural Language Process. (EMNLP)*, 2017.
- [19] J. Wangni, J. Wang, J. Liu, and T. Zhang, “Gradient sparsification for communication-efficient distributed optimization,” in *Advances Neural Inf. Process. Syst. (NeurIPS)*, 2018, pp. 1299–1309.
- [20] Y. Lin, S. Han, H. Mao, Y. Wang, and W. J. Dally, “Deep gradient compression: Reducing the communication bandwidth for distributed training,” in *Int. Conf. Learn. Represent. (ICLR)*, 2018, pp. 1–13.

- [21] M. M. Amiri and D. Gündüz, "Machine learning at the wireless edge: Distributed stochastic gradient descent over-the-air," *IEEE Trans. Signal Process.*, vol. 68, pp. 2155–2169, Mar. 2020.
- [22] M. M. Amiri and D. Gündüz, "Federated learning over wireless fading channels," *IEEE Trans. Wireless Commun.*, vol. 19, no. 5, pp. 3546–3557, May 2020.
- [23] A. Abdi and F. Fekri, "Quantized compressive sampling of stochastic gradients for efficient communication in distributed deep learning," in *Proc. AAAI Conf. Artif. Intell.*, Apr. 2020, pp. 3105–3112.
- [24] X. Fan, Y. Wang, Y. Huo, and Z. Tian, "Communication-efficient federated learning through 1-bit compressive sensing and analog aggregation," in *Proc. IEEE Int. Conf. Commun. Workshops (ICC Workshops)*, June 2021, pp. 1–6.
- [25] C. Li, G. Li, and P. K. Varshney, "Communication-efficient federated learning based on compressed sensing," *IEEE Internet Things J.*, vol. 8, no. 20, Oct. 2021.
- [26] J. P. Vila and P. Schniter, "Expectation-maximization Gaussian-mixture approximate message passing," *IEEE Trans. Signal Process.*, vol. 61, no. 19, pp. 4658–4672, Oct. 2013.
- [27] J. Mo, P. Schniter, and R. W. Heath, Jr., "Channel estimation in broadband millimeter wave MIMO systems with few-bit ADCs," *IEEE Trans. Signal Process.*, vol. 66, no. 5, pp. 1141–1154, Mar. 2018.
- [28] J. J. Bussgang, "Crosscorrelation functions of amplitude-distorted gaussian signals," *MIT Res. Lab. Electron. Tech. Rep.* 216, no. 5, 1952.
- [29] Y. LeCun, C. Cortes, and C. Burges, "The MNIST database of handwritten digits," [Online]. Available: <http://yann.lecun.com/exdb/mnist/>
- [30] D. P. Kingma and J. Ba, "Adam: A method for stochastic optimization," arXiv:1412.6980v9 [cs.LG], Jan. 2017 [Online] Available: <https://arxiv.org/abs/1412.6980>
- [31] Y. C. Eldar and G. Kutyniok, *Compressed Sensing: Theory and Applications*, Cambridge, U.K.: Cambridge University Press, 2012.
- [32] S. P. Lloyd, "Least squares quantization in pcm," *IEEE Trans. Acoustics, Speech and Signal Process.*, vol. 28, no. 2, pp. 129–137, Mar. 1982.
- [33] L. Schuchman, "Dither signals and their effect on quantization noise," *IEEE Trans. Commun. Tech.*, vol. 12, no. 4, pp. 162–165, Dec. 1964.
- [34] U. S. Kamilov, V. K Goyal, and S. Rangan, "Message-passing de-quantization with applications to compressed sensing," *IEEE Trans. Signal Process.*, vol. 60, no. 12, pp. 6270–6281, Dec. 2012.
- [35] S. Jacobsson, G. Durisi, M. Coldrey, U. Gustavsson, and C. Studer, "Throughput analysis of massive MIMO uplink with low-resolution ADCs," *IEEE Trans. Wireless Commun.*, vol. 16, no. 6, pp. 4038–4051, Jun. 2017.
- [36] L. Jacques, K. Degraux, and C. D. Vleeschouwer, "Quantized iterative hard thresholding: Bridging 1-bit and high-resolution quantized compressed sensing," arXiv:1305.1786 [cs.IT], May. 2013 [Online] Available: <https://arxiv.org/abs/1305.1786>
- [37] D. Guo and S. Verdú, "Randomly spread CDMA: Asymptotics via statistical physics," *IEEE Trans. Inf. Theory*, vol. 51, no. 6, pp. 1983–2010, Jun. 2005.
- [38] M. Bayati and A. Montanari, "The dynamics of message passing on dense graphs with applications to compressed sensing," *IEEE Trans. Inf. Theory*, vol. 57, no. 2, pp. 764–785, Feb. 2011.
- [39] S. Rangan, "Generalized approximate message passing for estimation with random linear mixing," in *Proc. IEEE Int. Symp. Inf. Theory (ISIT)*, Aug. 2011, pp. 2168–2172.x
- [40] S. M. Kay, *Fundamentals of Statistical Signal Processing: Estimation Theory*, NJ: Prentice Hall, 1993.